7-2023

TiO2 Coating Methods on Sb2O3 and Their Use as Anode Material in Lithium-Ion Batteries

Kithzia Czarina Gomez
The University of Texas Rio Grande Valley

TiO_2 COATING METHODS ON Sb_2O_3 AND THEIR USE AS ANODE MATERIAL IN LITHIUM-ION BATTERIES

A Thesis

by

KITHZIA CZARINA GOMEZ

Submitted in Partial Fulfillment of the

Requirements for the Degree of

MASTER OF SCIENCE IN ENGINEERING

Major Subject: Mechanical Engineering

The University of Texas Rio Grande Valley

July 2023

TIO_2 COATING METHODS ON SB_2O_3 AND THEIR USE AS ANODE MATERIAL IN LITHIUM-ION BATTERIES

A Thesis
by
KITHZIA CZARINA GOMEZ

COMMITTEE MEMBERS

Dr. Mataz Alcoutlabi
Chair of Committee

Dr. Ali Ashraf
Committee Member

Dr. Javier Ortega
Committee Member

July 2023

ABSTRACT

Gomez, Kithzia C., TiO_2 Coating Methods on Sb_2O_3 and their use as Anode Material in Lithium-Ion Batteries. Master of Science in Engineering (MSE), July, 2023, 57 pp., 35 figures, references, 70 titles.

The following thesis is concentrated on the development of $TiO_2Sb_2O_3$ composite material through the hydrolysis of $TiCl_4$ to be applied as anode material for lithium-ion batteries. Antimony (Sb) has been a material of interest due to its high capacity and good chemical properties. The TiO_2 accommodated the harsh volume expansion that Sb encounters during the alloying process while still preserving the high capacity offered by Sb. Its electrochemical performance exhibited a stabilized capacity of 523 $mAhg^{-1}$ after reaching 40 cycles with a capacity loss of 2.4% till reaching 100 cycles. High reversible capacity characteristics were present with an initial capacity of 427 mAg^{-1} at a current density of 50 mAg^{-1} in the first 10 cycles and finished with a capacity of 336 mAg^{-1}. Results displayed that there was good contact between the electrode and electrolyte having well distribution of electrons and ions. Overall, its preparation, characterization, and performance were studied for each ratio prepared to see its significance on the electrochemical performance.

DEDICATION

This is dedicated to my family who know me better than I know myself. To my mother, Patricia Gomez, for always being my best friend and having her best interests in mind. My father, Conne Aaron Gomez, for instilling in me a strong work ethic and morality. My sister, Zipacthly Aglaee Gomez, who unconsciously taught me to persevere and stay strong-willed. And lastly John Daniel Carrillo, I wouldn't have pulled through without your support and love in this chapter of my life. I love you all very much, my success is all devoted to you.

To my niece and nephew, Alezandra Anzaldua and Abdiel Perez, never desist from your dreams. All things are possible through hard work and commitment and that will lead us closer to our desired victories.

ACKNOWLEDGMENTS

The authors acknowledge the support from the NSF PREM program under Award DMR-2122178: UTRGV-UMN Partnership for Fostering Innovation by Bridging Excellence in Research and Student Success.

TABLE OF CONTENTS

Page

LIST OF FIGURES

Page

CHAPTER I

INTRODUCTION

Electricity has taken over all energy systems and permitted existence to play smoothly; that it would be hard to imagine the absence of this luxury. Electricity was established when an electrochemical cell device got invented, well known as a battery that allows the energy from a chemical reaction to be converted into usable electricity [1]. It began with a disagreement between the findings of two physicists, Luigi Galvani and Alessandro Volta, in the eighteenth century. Where Galvani believed that animals could generate electricity while Volta debated that it was because of the “voltaic pile”. It was constructed of zinc and silver disks separated by a cloth soaked in sodium chloride solution [2]. The dissimilarity of both concepts paved the way to developing a battery since in the aspect of Galvani he was looking into bioenergy and Volta into energy storage.

In 1866, the previous work led to a French engineer named Georges-Lionel Leclanhe to take interest on the topic and built a battery based on zinc (negative electrode-anode) and a manganese oxide-carbon mixture (positive electrode-cathode) with ammonium chloride (electrolyte) which rose to become the prototype to the current zinc carbon cell used today [3]. Afterwards came the invention of rechargeable batteries and brought along the concept of redox reactions yet not much occurred subsequently. At that moment every device was effective and

meeting all needs. Until the late 1960s, innovations took place and current technology had to be updated.[4] This period is relevant to what is occurring now. Our electronic devices, transportation and energy storage devices are frequently changing causing to look for the latest material or technique. Interestingly, electrical and combustion engines competed in the 19-20th century, but due to the sightings of more petroleum being available, combustion won.[3] However, batteries are still as important in vehicles as it is applied as a starter battery.

With the rapid progress seen in nanotechnology it has been significant in the development of new battery materials. Targeting on understanding and manipulating the physical and chemical properties of materials at a nanoscale.[5] Anode materials specifically to improve the capability and create innovative approaches such as (1) designing nanostructures for better diffusion, (2) apply nanocoating to subside side reactions, and (3) mix with conductive materials.[6] A lot of these systems have been used in current products or still in the testing phase.

The battery field has grown tremendously especially with LIBs taking over a variety of applications since its outbreak in the early 1990s.[7] They have continuously been worked on for the past 25 years, yet just recently it has attracted a large audience to perform research. Exclusively with the successes of solid-state batteries, sodium-ion batteries (SIBs), and development of potential anode materials. The state of the art of electrode materials has a substantial role to revolutionize all consumer applications. In the case for electric vehicles, nanotechnology has triumphally taken a role in incorporating lithium titanates, silicon nanocomposites, or nanocoating to accommodate with EV applications.[8] Other advancements in the battery industry have been integrating nanostructured materials such as metal oxides, alloys, and nano-carbons[9-11] through a variety of methods such as electrospinning, carbon-

coating, hydrothermal method.[12-14] This results in more commercial success and opportunities for the society.

The following work will focus on TiO_2 /Sb_2O_3 nanocomposite to investigate its performance on lithium-ion batteries (LIBs) as a potential anode composite material to replace current material. Various concentrations of Sb_2O_3 were coated on TiO_2 to analyze the effect on its electrochemical performance. The depth of its synthesis, characterization and electrochemical performance will be discussed.

CHAPTER II

LITERARY REVIEW

2.1 The Importance of Battery Technology

Efforts to uncover effective strategies to replace fossil fuels and current energy sources have been significant for the battery research community. Especially since it has become a challenge to decrease the aftermath of CO_2 emissions now that it has doubled from 1970 to 2005. [15] The urgency to adopt a sustainable environment has been detected. Examples such as Deng et al. is using nanostructured TiO_2 and Sn-based materials in LIBs since

This wide increase in energy consumption in many sectors reflects the country's economic growth due to the advancements in technology.[16] These are electronic devices, electric vehicles (EVs), and stationary storages of electric power. Batteries have become a key role in transitioning technology since they are known to have the highest charge density in such a compact system.[17] They can efficiently store and deliver energy at a high return factor; guaranteed to be more than conventional batteries.[18-20] Standard LIBs use synthetic graphite such as MCMB (mesocarbon microbeads) as their promising carbon anode electrode which typically has a theoretical specific capacity of 372 mAhg-1 and displays less than 10% volume change during testing. [17, 21] It's been the main anode material since 1991 but due to its limited

capacity and dendrite deposition resulting in safety issues[22, 23], there have been multiple studies on discovering alternative anode materials for LIBs. Especially targeting those that are abundant and show enhanced properties that can outperform current batteries and keep up with the energy market.[24, 25] Research on LIBs has expanded rapidly over the past decade. According to the Global Market, money invested on LIB research was USD 65.9 billion in 2021 and is expected to grow exponentially to USD 273.8 billion by 2030.[26]

The success of lithium-ion batteries paved the way for the development of sodium-ion batteries (SIBs), lead-acid batteries, and much more. SIBs have been identified as a great alternative to LIBs due to its abundancy and being inexpensive.[27] These advancements are expected to develop the ideal battery, which is having high power density and specific energy with a long cycle life that won't be costly.

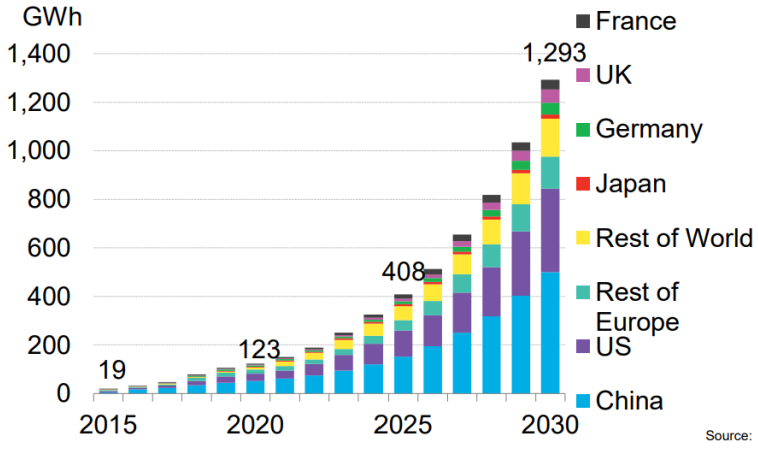

Figure 1. Expected demand for LIBs through time [26]

2.2 Components of a Lithium-Ion Battery

A LIB is comprised of the following main components: cathode, anode, electrolyte, and a separator. The interactions that occur within these components decides the specifics of its performance, life durability, and safety. Which is why material selection is crucial.

Batteries have two electrodes which are identified as the anode and cathode. The anode is distinguished as the negative electrode, where oxidation occurs. An anode is fabricated of composite material and placed on copper foil which operates as the current collector. And the cathode is the positive electrode where reduction takes place. Both electrodes (anode and cathode) store lithium ions through intercalation.

Batteries also have a separator which is positioned in between both electrodes to prevent contact which can lead to short circuiting and potential explosions. When assembled, the separator gets wet with the electrolyte and forms a catalyst which will promote lithium ions to move in between the electrodes.[28] Although separators collect no electrical conductivity as ions as passing freely they have an important role towards the safety of the battery.

Early separators were established of cellulose, rubber, glass fibers, and polyethylene plastic. Very early on, it was convinced that wood was the best material but it would deteriorate in electrolyte.[29] Current commercial LIBs use polyolefin for separators due to demonstrating excellent mechanical properties and stability and its affordable cost. Even with deciding a material it must be absorbent and permeable with a pore size along 30-100 nm. This is so it can carry enough electrolyte and act out when the cell overheats.

Electrolyte is a substance that can conduct electricity when mixed with a solvent. It is a mixture of organic carbonates and lithium salt.[30] The salt provides the lithium ions that will be traveling between the electrodes and the carbonate as the solvent for a protective layer. [31] This movement across is what represents the discharge and charge providing electrical current. Electrolytes are seen in different forms: liquid, gel, and solid depending on the application. During the development of LIBs, electrolyes were dependent on the chemistry of the cathode. In 1972, ether-based electrolytes were utilized when TiS_2 was the cathdoe material. Yet when Goodenough discovered that transition-metal oxides had high voltage and potential cathode material characteristics , there was a shift from using ethers to esters.[32] An ester group involves two carbon atoms and two oxygen atoms attached by double bonds. They are formed under the combination of an organic acid and an alcohol and resulting in a second bypdroduct, a water molecule. Generally ethylene carbonate (EC) and propylene carbonate (PC) were used but PC was often favored because of its stability at high voltages (> 4.0 V). Yet the usage of EC electrolytes combined with graphite increased energy density in LIBs by 30-50% compared to early versions of batteries using carbon anodes. [33]

Based on Wang et al.[34] lithium difluorophosphate (LiDFP) was tested as as an electrolyte additive for LIBs. LiDFP being a decomposition product of $LiPF_6$, which is what is applied on our batteries, were seen to enhance its rate and cycablity performance of tested batteries with a capacity retention of 92.6% after 100 cycles. This acts as evidence that with the attribution of $LiPF_6$ it helped to modify the surface of the anode and cathode leading to improved

performances of batteries. This confirms that the electrolyte's performance is linked to the electrode material that its interfacing with.

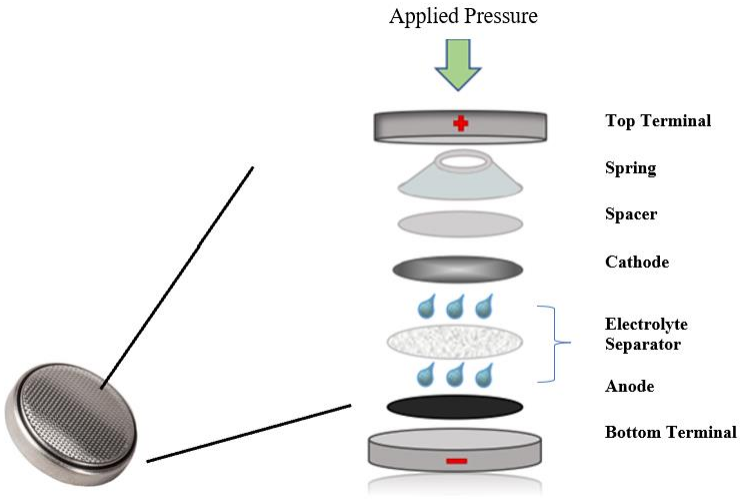

Figure 2. Schematic Image of a Lithium-ion Battery

2.3 Working Principle of Lithium-Ion Batteries

Electrochemistry concentrates on the movement of materials that conduct electricity that being atoms and electrons reacting. Lithium-ion batteries fall into this realm since carbon, oxygen, and electrons are all present while a battery is running.

When charging a battery, electrons are traveling from the cathode to the anode yet when discharging, it will switch, and it will travel from the positive electrode (anode) to the negative electrode (cathode). During this time ions will travel back and forth between the anode and cathode through the electrolyte. Since electrons are interchanging between both electrodes, their charges will change. Therefore, when charging electrons will leave the negatively charged

cathode, which will make it positive and will travel through a current collector to reach the current positively charged anode, which will eventually become the negative electrode.

This is the phenomena seen in LIBs known as the rocking chair principle. It is built around the concept of Li^+ traveling back and forth between both electrodes like a rocking chair, this analogy was propped by Armand around the 1970s.[35] During this intercalation, batteries experience redox reactions known as reduction and oxidation. The following equations below demonstrate the reversible reactions that occur within a LIB while intercalating.

Anode: $6C + xLi+ + xe- \leftrightarrow LixC6$ (1)

Cathode: $LiCoO2 \leftrightarrow Li1-x\ CoO2 + xLi+ + xe-$ (2)

During oxidation, batteries lose electrons and in reduction batteries gain electrons. The exchanging of electrons is what creates electricity. Both the anode and cathode have a very distinguished relationship. They create a lattice framework leaving zones where lithium-ions can fill into the gaps.

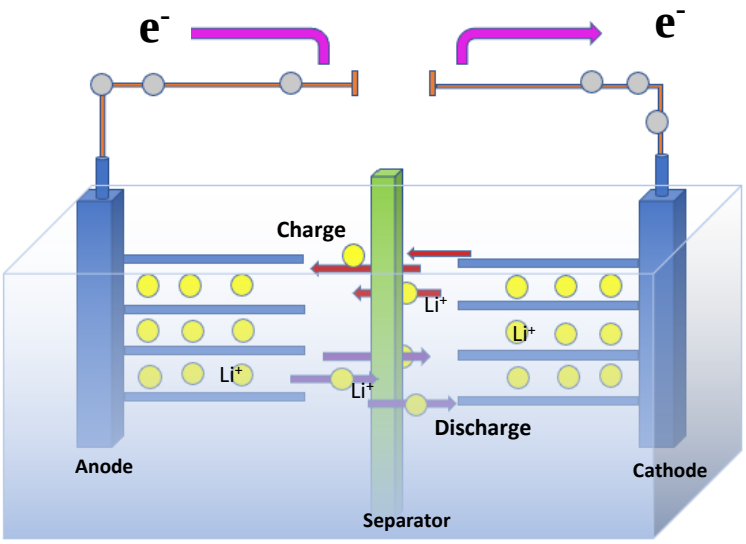

Figure 3. Lithium-ion Battery Working Principle

2.4 Degradation Seen in Batteries

Understanding and knowing what occurs inside a battery is critical to identifying what the pinpoint problem is and create cost effective solutions. This subject is challenging to master. Having these mechanisms occurring creates a drawback on high-capacity electrodes. Due to the nature of these reactions the best method to examine this is through the usage of *in-situ* and *ex-situ* characterization techniques to observe the surface. That being X-ray diffraction (XRD), transmission electron microscopy (TEM), atomic force microscope (AFM), X-ray photoelectron spectroscopy (XPS) and scanning electron microscope (SEM). Typical degradation situations seen in LIBs causes capacity loss and fading and this due to the mechanical and chemical changes occurring inside. Various approaches have been directed on LIBs to mitigate these issues, such as surface coating and adding buffers. These degradation mechanisms are generally better understood in LIBs with graphite as its desired anode material. Below will be discussed few failure mechanisms that are continuously seen in LIBs.

2.4.1 Lithium Plating

Lithium plating occurs on the negative electrode as its being run by a current. It begins at the initial stages as the electrode is making its first contact with the electrolyte. Metallic lithium collects along the surface of the negative electrode instead of traveling through it. And this process of depositing occurs faster than it intercalates. Based on Campbell et al.[36] work, techniques were discovered to observe lithium plating based on voltage analysis to quantify the plating. Further work is required to fully understand the influence between capacity and charge owing to the plating occurring. Disadvantages are causing a short circuit from either getting the separator punctured or the metal deposits into the separator because of compression.[37] Another consequence from lithium plating is it conducts other side reaction, that being

developing the SEI layer. The lithium that gets plated becomes “dead lithium” and becomes a thick layer which comes to further be an SEI layer. Cell models have been used to simulate defects on the cells and analyze the changes that occur.

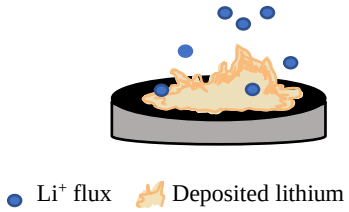

Figure 4. Lithium Plating in lithium-ion batteries

2.4.2 Volume Expansion

Result of volume expansion degradation mechanism will lead to a loss of electrolyte which will dry all local areas where transportation occurs leading to dried pores. Then subsequently losing active material in both electrodes. A linkage of this action is a particle fraction that can possibly occur in both electrodes from the occurring volume change leading to a mechanical failure. This phenomenon is seen in high-capacity materials like silicon. One method to enable these large changes has been surface coating. Riley et al.[38] applied a alumina surface coating on MoO_z LIBs through atomic layer deposition (ALD). Results showed that the coating benefited the performance by achieving a stable capacity of 900 $mAhg^{-1}$ for 50 cycles at C/2 scan rate. In comparison to those bare and coated, the coated created an adhesion factor demonstrating less mechanical degradation and volume contractions.

2.4.3 SEI Layer Growth

The solid electrolyte interphase (SEI) is one of the main degradation modes that occur in most of all batteries. This process occurs along the negative electrode surface when the electrolyte makes contact. This mechanism appears at the beginning of testing usually on the first cycle when it is operating at low voltages. As it is occurring, redox reactions irreversibly break down the electrolyte leading to a loss of quantity and gets collected on the negative electrode surface. Because of the SEI layer it automatically results a 10% drop in capacity at least, and as the battery is being tested and aging the SEI layer will get thicker. The growth of the SEI layer can be from multiple reasons: (1) as the SEI gets established diffusion gets difficult and collects at the surface, and (2) there are various materials that side-react with the electrolyte causing SEI growth.[39] It can be classified that the growth rate of the SEI layer is correlated with the square root of time. Meaning that as the SEI is getting thicker the diffusion rate of ions will ultimately get slower.[40] This reduces the electrochemical stability of the electrolyte at high current values. With this loss of stability side reactions are prone to occur. Therefore, at a certain thickness, the anode's ability to absorb lithium ions will reduce and get deposited into the surface instead. However, there is positive feedback of this failure in its early stages acting as a safety measure. It helps by allowing Li ions to transport and block electrons to avoid extra electrolyte corrosion and maintain the battery cycling.[41] During the first cycle its performance is not affected until afterwards.

2.5 Anode Materials Used in Lithium-Ion Batteries

Graphite is the most used commercial anode material for LIBs due to its abundancy, great electrical conductivity, and rate stability with a theoretical capacity of 372 $mAhg^{-1}$.[42] Yet with upcoming technologies and need of increased capacity and storage there has been a high interest in modifying the anode material. Current work has been downscaling from conventional bulk material to a nanoscale as an approach to increase storage capacity. Nanda et al.[43] detected that a decrease in the particle size substantially improved the distribution of ions and electrons. Other methods have been incorporating high-capacity anode materials as supplementary material to boost the capacity of current batteries. Alloy-type electrodes made of semi-metals and metals which form intermetallic phases when reacting to metal-ions are favorable because there's a smaller influence on lithium plating compared to graphite.[44] Examples of high-capacity materials are Si, Ti, Sn and Mg to name a few. Along the interested materials, the alloy between LTO (lithium-titanium-oxide) has been recognized and drawn to attention. Advantages compared to graphite is that the volume change is trivial, it assembles a thin SEI layer or none therefore leading to no lithium plating. Silicon (Si) is also another widely explored anode material demonstrating a pure theoretical capacity of 3579 $mAhg^{-1}$, which is significantly higher than conventional graphite when forming amorphous Li.[45]Due to its high capacity many applications have been discussed such as adding new binders, changing the electrolyte, and applying additives.[46] Now even though Si has a larger gravimetric capacity, 3572 $mAhg^{-1}$, than of Sn being 992 $mAhg^{-1}$ their volumetric capacities are similar to each other (7254 mAh cm^{-3} for Sn and 8322 mAh cm^{-3} for Si) at full lithiation.[47]Another material utilized is Ti, because of its well thermal stability compared to commercial graphite.

But the biggest issue with inserting high-capacity materials is it causes a large amount of volume expansion during lithiation/delithiation which results in degradation and capacity loss. It can substantially reorganize the anode material's atoms and upbrings unstable issues and the formation of SEI. This is just one method to mitigate this issue, which is why this topic is explored to develop a strategy.

A great candidate for an anode material in lithium-ion batteries is antimony. It is highly recognized due to its diversity on being used for both lithium-ion batteries and sodium-ion batteries. Sb-based alloys have been the most interesting since pure Sb presents a high theoretical capacity of 660 $mAhg^{-1}$, which is several times higher than traditional graphite.[48] Also due to its puckered layered structure and interlamellar spacing, it displays a high conductivity of $2.56X10^{6}$ and a density of 6.68. Because of its layered shape, it can adjust itself during the insertion of lithium ions.[49] But significantly, Sb is definitely an attractive anode material because while alloying with Li^{+} it undergoes simpler steps compared to group 4 known as the crystallogens (Sn, Ge, and Si) based off of work by Liang et al.[50] This can be supported by recognizing that few intermediate phases are established in the charge/discharge cycles. Also, Sb compared with its family elements (Group 5) such as Phosphorus has not shown excellent reversibility and initial coulombic efficiency.[51] This is based on work incorporating P-graphene, P-porous carbon, and P@CNTs as anode material.[52, 53] Other methods supporting Sb have been creating hollow and nano-sized structures[54-56] and applying buffer matrices.[57, 58]A unique Sb-alloy material is antimony trioxide (Sb_2O_3). It exhibits a theoretical capacity of 1109 $mAhg^{-1}$ with great structural stability. Yet the challenge is displaying its full theoretical capacity. Work using Sb_2O_3 as a potential anode material has received great results. Work such by Tan et al.[59] effectively synthesized bundle-shaped Sb_2O_3 through thermal annealing and it

astonishingly exhibited 594.1 $mAhg^{-1}$ after 40 cycles at a current density of 20 mAg^{-1}. Liu et al.[60] fabricated a polymeric binder forming a CMC-FA@Sb_2O_3 anode material for LIBs and it presented a specific capacity of 611.4 $mAhg^{-1}$ after 200 cycles at 200 mAg^{-1}. Both investigation Yet a large setback of Sb is that when undergoing intercalation, forming Li3Sb, it contributes to a large volume expansion of approximately 137%. [61] This volume change which is pertained from the alloy reaction can result in a large capacity fade as its testing since there is an action of collapsing occurring in the anode.[62]

The following reversible alloying reaction of Sb_2O_3 as the anode material is shown in Eqs. 1 and 2.[63]

$$Sb2O3 + 6Li+ + 6e- \rightarrow 2Sb + 3Li2O \quad (1)$$

$$2Sb + 2xLi+ + 2xe- \rightarrow 2LixSb, x \leq 3 \quad (2)$$

Now Sn and Sb are along the same period of the periodic table (row 5)[64] indicating that Sb has a smaller atomic radius than Sn therefore Sb will experience less volume change. Based on Darwiche et al.[65] bulk Sb was tested and compared in Li and Na-ion systems. It was observed that Sb underwent unknown alloying mechanisms in Na compared to Li. In the case with Li, Sb undergoes an alloying/dealloying process whereas with Na it's not fully comprehendible since it goes through complex stages. Those being of amorphous intermediate phases present at the former but not for the latter. Latter being a critical point where conversions are taken in place reconstructing the electrode material. Yet compared to Li, these phases are expected based on the phase diagram.[66] Furthermore, the electrochemical performance of Sb and Na outperformed Li and it can assumed that it was due to the decrease on volume expansion when converting Sb (181.1 $Å^3$) to hexagonal Na_3Sb (237 $Å^3$).[67] According to calculations from He et al.[49] the

strain relaxation is higher in a Na-Sb system than in a Li-Sb system which results to a slow diffusion and amorphous phases instead of intermediate.

Even though graphite has dominated numerous potential materials; with the rise of technology these candidates have surfaced back to be studied. It does seem reasonable to use these elements to reach a high energy density, but more information is required or else it will become worse than current graphite LIBs (that being like Si, Sb, and Sn).

The objective is to apply a coating of synthesized TiO_2 onto the surface of Sb_2O_3 nanoparticles via a hydrolysis and hydrothermal process. Performing hydrothermal synthesis can generate nanomaterials at high temperatures with the benefit of not losing a significant amount of material[68]. This is one of the main influences why it's used over other methods.

The advantages of using TiO2 with other anode materials can expected is: (i) having a good distribution of TiO2 particles across the matrix which can act as a buffer to relieve the volume expansion occurring during charge/discharge cycles, and (ii) achieving low irreversible capacity loss during the first cycle and (iii)and maintain the anode stability without carbon coating.[61]

Therefore, incorporating TiO_2 with Sb_2O_3 will provide some benefits especially against volume expansion, but some will be sacrificed due to its low theoretical capacity.

CHAPTER III

LABORATORY INSTRUMENTATION

3.1 Equipment for Material Preparation

To properly examine the use of Sb-based nanocomposite as a potential anode material for lithium-ion batteries, the following equipment and software's were used to aid in the whole investigation process.

3.1.1 Fiberio Forespinning Machine

A process known as Forcespinning (FS) established by Karen Lozano and Kamal Sarkar at the University of Texas Rio Grande Valley became extraordinary and a great asset to the nanotechnology department. It develops nanofibers based off a variety of targeted materials. This method incorporates centrifugal forces while similar techniques use electrostatic forces.[69] Parameters to keep in mind when maintaining the morphology of developed fibers is preserving

its rotational speed, which is set to its desired point, and the uncontrolled factors being temperature and humidity of the room.

Figure 5. Cyclone Forcespinning Machine

3.1.2 Heat Treatment Furnaces

The following heated furnaces used was the OTF-1200X tube furnace developed by MTI Corp. California, USA, to perform calcining and carbonization thermal treatments under air or argon. And secondly the Isotemp 285A vacuum oven by Fisher Scientific to dry prepared samples and remove unnecessary solvent.

Figure 6. Thermal treatment equipment: (a) OTF-1200X Tube Furnace and (b) Isotemp 285A Vacuum Oven

Figure 7. Vacuum Oven

The following oven demonstrated on Fig.7 is used to store all synthesized material under vacuum. This ensures that no moisture is collected which can be destructive and reflected on the performance.

Figure 8. Distillation set-up

3.1.3 Battery Assembly Equipment

All lithium-ion batteries are prepared using equipment seen on Fig 8. The MBraun Glovebox is crucial to be kept under maintenance with the parameters of pressure: 5-9 mbar, H_2O: 1.8 ppm, and O_2: <0.5 ppm. The hydraulic crimping machine is operated to properly seal coin cells at approximately 1000 psi.

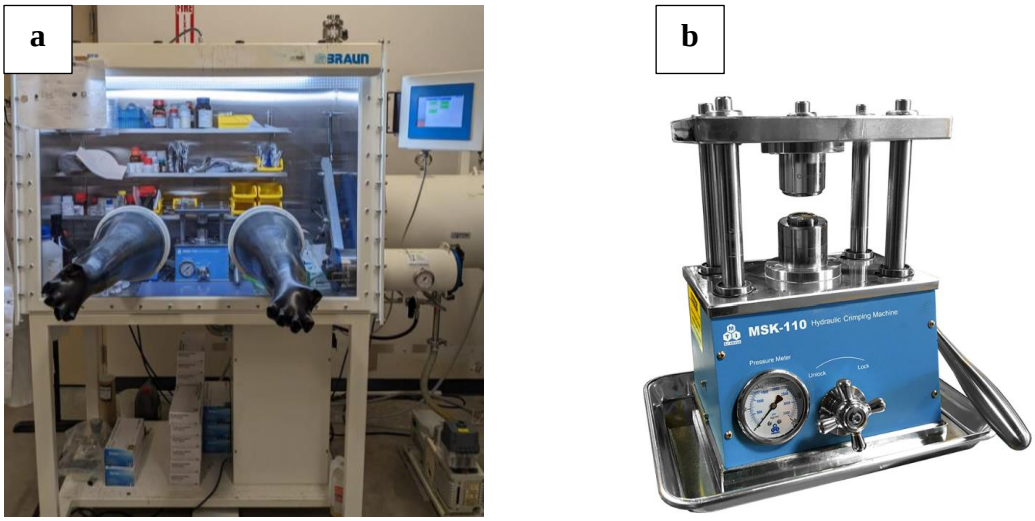

Figure 9. Equipment to assemble lithium-ion batteries (a) MBraun Lab Star Pro Glove Box and (b) MSK-110 Hydraulic Crimping machine by MTI Corporation

3.2 Characterization Equipment

3.2.1 Morphology Characterization

Both SEM and EDS microscopes were operated to study the surface and morphology of desired material. SEM is supplied with a EDAX detector provided by Mahwah, NJ, USA.

Figure 10. Sigma VP Carl Zeiss Scanning Electron Microscope (SEM) paired with Energy-Dispersive X-ray Spectroscopy (EDS)

3.2.2 X-ray Photoelectron Spectroscopy

The XPS is provided by Thermo Scientific and is equipped with a K-Alpha photoelectron spectrometer. The following piece of equipment was used for elemental identification and study the depths of the material for overall coating measurement.

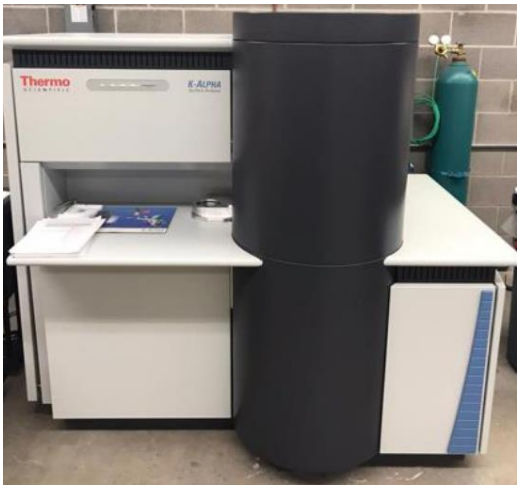

Figure 11. X-Ray Photoelectron (XPS) Machine

3.2.3 Electrochemistry Battery Testing Systems

Autolab spectroscope is controlled with a computer that is equipped with Nova 1.10 software. Test measured is electrochemical impedance to study the internal ohmic resistance and reactance that is occuring in a lithium-ion battery as current is applied. Measurements help to identify the battery's cycle life and early signs of weakness.

Figure 12. Autolab 128N Electrochemical Impedance Spectroscope

CV testing is provided by the Biologic instrument. Where oxidation/reduction reactions are displayed as it is being scanned at a rate of 0.2 mV/s between 0-3 V at a frequency of 0.1 Hz. These measurements justify the diffusivity of Li^+ ions and intercalation reactions. The following equipment is controlled with a computer that is equipped with the BTLab software

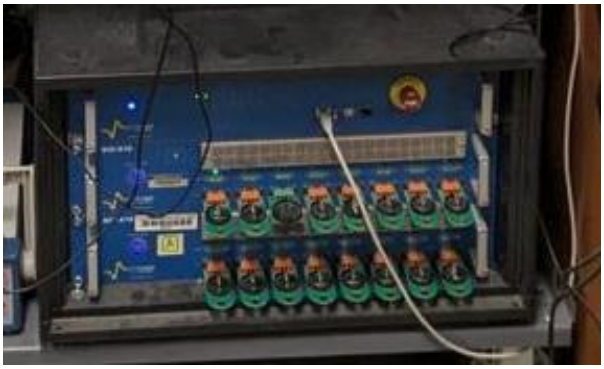

Figure 13. Biologic Cyclic Voltammetry (CV) Instrumentation

Rate performance is computed from Arbin testing system where batteries are analyzed to test its stability and capacity retention across different current densities that are based on the anode's weight. Current densities at 50, 100, 200, 400, and 500 mAg^{-1} and a potential range of 0.01-3 V. This instrumentation is monitored through a computer that is equipped with MITS Pro software.

Figure 14. Arbin Testing System

To study its cycle performance as its charging/discharging the Lanhe battery testing system was utilized. It measures the specific capacity as its intercalating on set number of cycles across a voltage of 0.05-3 V. This system is connected to a computer that is equipped with LAND Battery Testing System software.

Figure 15. Lanhe Testing System

3.3 Fabrication Techniques

Material was fabricated in multiple methods, temperatures, and material composition percentages to identify which process was significantly better on influencing its electrochemical performance. Methods were distillation and applying an annealing process at 175 °C compared to it bare. Second is a hydrolysis/hydrothermal treatment at 175 °C and thirdly forespin precursor fibers and develop calcined material.

3.3.1 Preparation of Annealed Material: Method 1

1g of Sb_2O_3 was weighed and a 250 mL solution of $TiCl_3$ and $NaCH_3CH_2OO$ was prepared at a concentration of 0.166 M. Subsequently the measured Sb_2O_3 was added to the prepared solution and onto a round bottom flask for distillation. The rate of air was controlled at 100 mL/min and was constantly heated to 100 °C for 8 hours. Samples afterwards were cooled

down to room temperature and washed/filtered with DI water. For annealed samples, an additional step was required after cooling down to room temperature. Samples were placed inside a muffle furnace at 750 °C for 1 hour to initiate the annealing process and cooled to room temperature subsequently.

3.3.2 Hydrolysis

In literature, hydrolysis is considered as a decomposition reaction that uses water as a reactant. Meaning that the chemical reaction occurring is due to a molecule of water breaking apart chemical bonds that make up the material and replacing it with itself.[70]

3.3.3 Preparation of Sb-coated Composite Material: Method 2

(3:1) $TiO_2Sb_2O_3$ material was synthesized through the hydrolysis of $TiCl_4$ followed by hydrothermal treatment at 175 °C. Water used was ultrapure 18 mega ohm Millipore water. The ratio of water to $TiCl_4$ was 30:1, a volume at 50 mL of $TiCl_4$ and 250 mL of water. The $TiCl_4$ was added to chill water under vigorous stirring in a 0.5 L three-neck round bottom. The water used was cooled in an ice bath prior. The $TiCl_4$ was added quickly to the water with the aid of an additional funnel. The solution was then placed into 23 mL autoclaves, which were filled up to 80% of the flask, for hydrothermal treatment. Each contained different masses of Sb_2O_3 to generate the appropriate ratio of TiO_2 to Sb_2O_3. In this case, being at a (3:1) ratio. The autoclaves were sealed and placed in an oven for 3 hours at 175 °C to begin annealing. Afterwards, a white precipitate was formed which was extracted from the Teflon bombs and washed with Millipore water. The washed, white precipitate was then dried in a 50 °C oven overnight to prepare it for characterization and use of application.

3.3.4 Preparation of Fiber Composites

Materials used to fabricate precursor fibers were polyvinylpyrrolidone (PVP) with a molecular weight of 1,300,000, absolute ethanol (200 proof) purchased from Sigma-Aldrich and Antimony (III) acetate precursor (97%) purchased from Alfa Aesar and used as is.

Microfibers were synthesized by calcinating the centrifugally spun precursors. Started by creating the fiber solution, which consisted of 3g of PVP dissolved in 17g of ethanol and was stirred until homogeneously. Once properly mixed, 1.5 g of Antimony (III) acetate was added to the same solution and mixed until reaching homogeneously again. Solution was centrifugally spun at a range of 4,500-5,500 rpm at a relative humidity below 60% to get a high yield of fibers. The following fibers were subsequently placed into the open tube furnace for calcination and were heat treated in air at 700 °C for 3 hours at a ramp rate of 2 °C/min, ending with pristine precursor fibers. Following material was grinded with a mortar and pestle and used to prepare slurry solutions as the baseline for comparison.

3.3.5 Fabrication of Sb-based Slurry Anodes

Solutions were made at an 8:1:1 composition ratio. Comprising of the active material, conductive carbon black, and selected binder respectively. In this case, 0.40g of synthesized $TiO_2Sb_2O_3$ (active material) was mixed with 0.05g of SuperP conductive carbon black and 0.05g of PAN. The solvent used was dimethyl formamide (DMF) and was determined dropwise and mixed under magnetic stirring for 24 h at room temperature until obtaining a homogeneous solution. If poorly mixed, it will not disperse evenly and offer good results. Once achieving homogeneity, solution was placed onto the copper foil. The copper foil was cut and placed onto a

metal plate and coated with ethanol. The solution was coated onto the copper foil utilizing a scraper and was controlled at a thickness of 10 microns. The slurry mat was placed inside the Isotemp vacuum oven for 24 h at 60°C. Once dried, the slurry was put inside an open tube furnace, OTF-1200X, to apply a heat treatment at 350 °C with a ramp rate of 2°C/min for 5h under an argon atmosphere. Afterward, the slurry was cut into 0.5” diameter discs and weighed to determine the amount of active material for when testing the anode.

All material synthesized followed this specific method, at the same ratio of 8:1:1 to prepare slurry solution and dried at 60 °C. Independent variables were heat treatment temperatures of 300 °C, 350 °C, and 400 °C each at a ramp rate of 2 and 3 °C/min.

CHAPTER IV

FINAL RESULTS AND DISCUSSION

4.1. Morphology and Characterization of Sb-Coated Nanocomposite Material

4.1.1 X-Ray Diffraction (XRD) Analysis

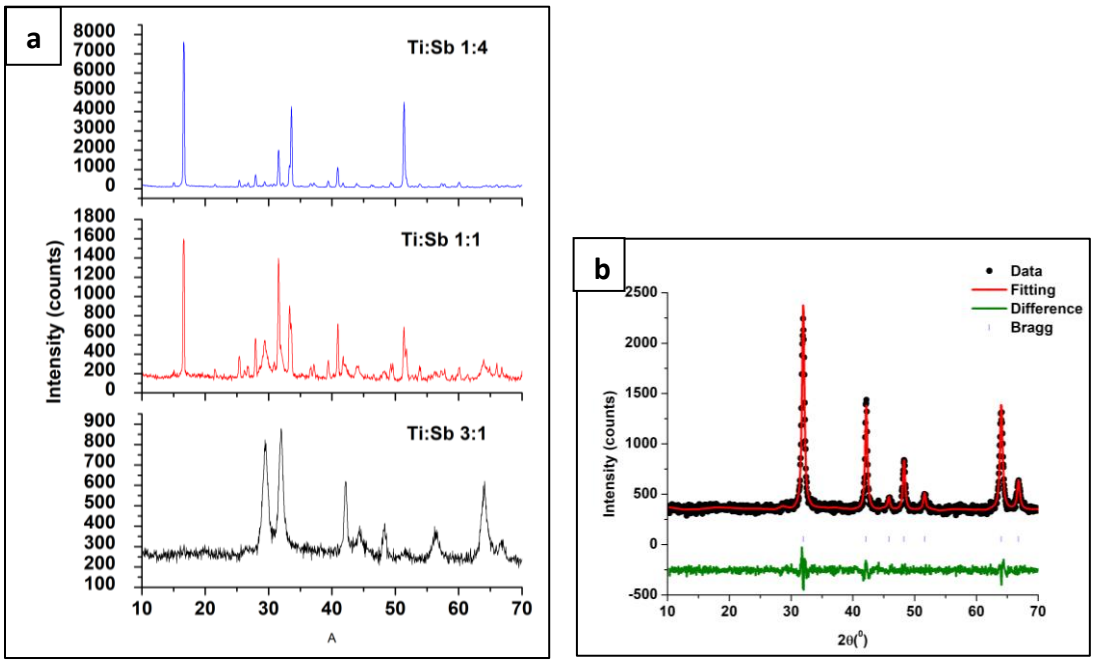

Figure 16. XRD analysis of (a) TiO_2/Sb_2O_3 at different composition ratios and (b) synthesized TiO_2

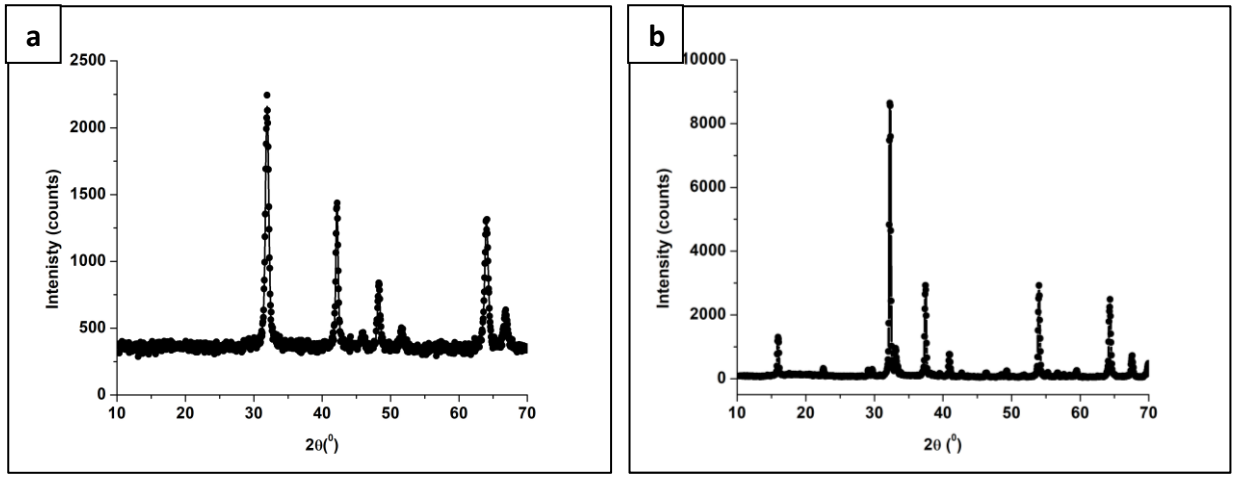

Figure 17. Non-fitted XRD spectrum of (a) synthesized TiO_2 and (b) Sb_2O_3

4.1.2 EDS/XPS Analysis

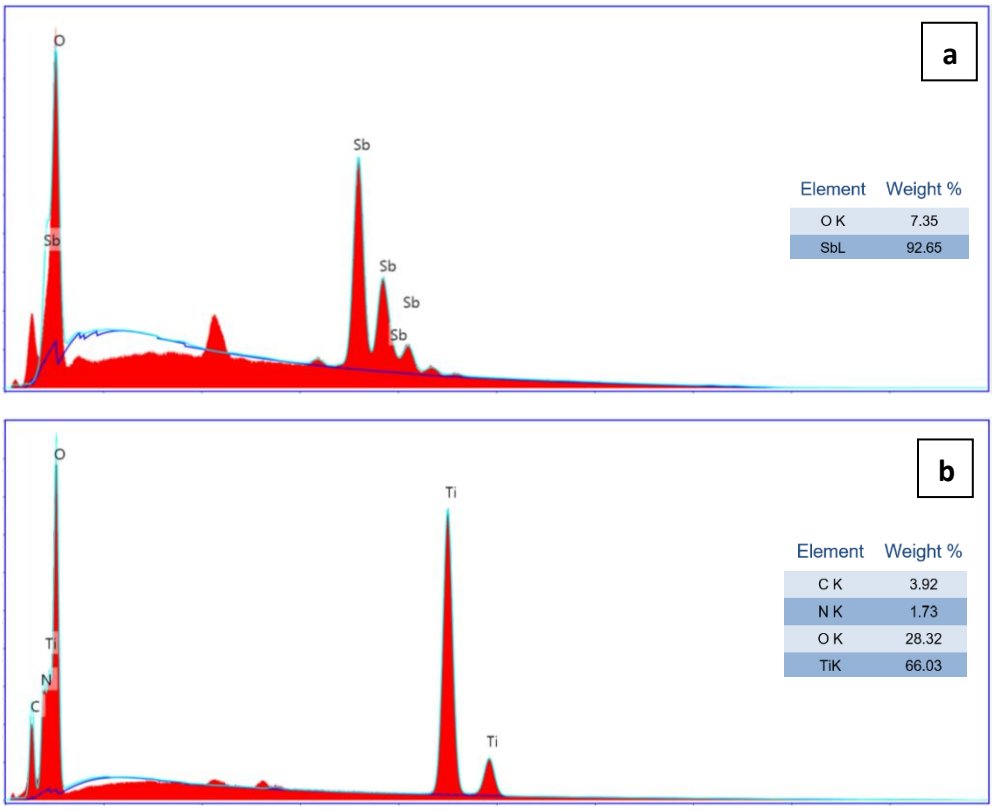

Figure 18. EDS spectrum of (a) Sb2O3 (b) TiO2 and (c) (3:1) TiO2/Sb2O3 material

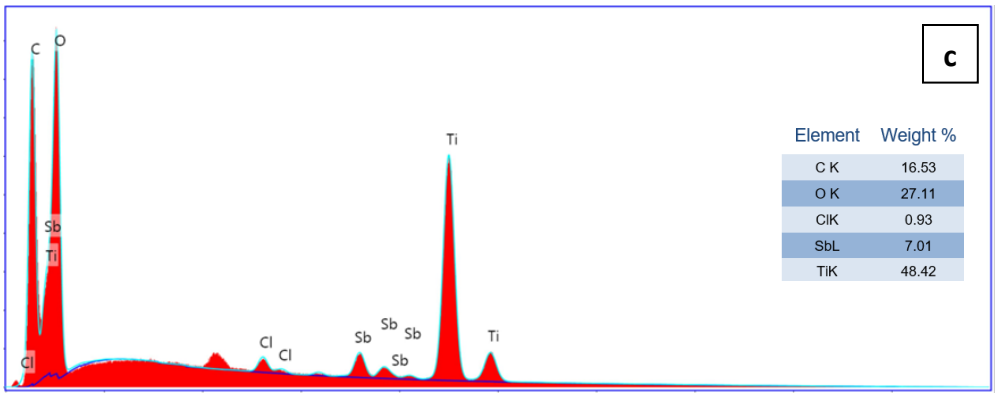

Figure 18, cont.

X-ray photoelectron (XPS) characterization was completed to measure and verify in what state the revealed materials are in the samples. Based on the XPS spectrums, the Sb present is represented as Sb (0) and Sb_2O_3, this is typically observed in the literature for Sb_2O_3.

Fig. 17 shows the XPS for the hydrothermally synthesized TiO2 nanoparticles at 175°C, included for reference. The XPS spectrum showed the presence of 3 peaks located at 458.6, 464.3 and 472.0 eV, which correspond to the Ti $2P_{3/2}$, $Ti2P_{1/2}$ and the Ti 2P satellite peak respectively. The peaks were determined to consist of individual peaks and no further deconvolution was necessary for the fitting. The observed peak energies are consistent with those observed in the literature for TiO_2 in the rutile phase. Fig. 20a shows the Ti 2P for the 1:1 TO_2 to Sb_2O_3 synthesis, which showed the same three peaks as the pure TiO_2 sample (fig. 19) located at 458.9, 464.6, and 472.3 eV. As with the TiO_2 nanoparticles these peaks observed in the TiO_2/ Sb_2O_3 composite nanoparticles were determined to be the Ti $2P_{3/2}$, $Ti2P_{1/2}$ and the Ti 2P satellite peak respectively. Similarly, the TiO_2 1 to 3 Sb_2O_3 synthesis in fig. 20b showed three peaks in the Ti 2P region located at 458.6, 464.3, and 472.0 eV. As with the other samples the Ti peaks correspond to the Ti $2P_{3/2}$, $Ti2P_{1/2}$ and the Ti 2P satellite peak respectively. Fig. 20c

showed the Ti2P XPS spectrum the for the 1 to 5 synthesis. The 1:5 synthesis was deconvolved into three peaks located at 459.2, 464.9, and 472.6, which correspond to the Ti $2P_{3/2}$, $Ti2P_{1/2}$ and the Ti 2P satellite peak respectively. As mentioned earlier these peaks are also consistent with TiO2 in the rutile phase.

Fig. 21 shows the Sb 3d and O 1S XPS spectrum for the 5 to 1, 3 to 1 and 1 to 1 Sb2O3 to TiO2 synthesis. The XPS spectrum from the 5:1 Sb2O3: TiO2 showed the presence of 4 peaks, which were further deconvolved into 5 peaks. The fifth peak is from the overlap of the O 1S spectrum with the Sb 3d spectrum. The binding energies of the individual peaks were located at 528.3, 530.7, 531.4, 537.7 and 540.3 eV, which correspond to the Sb (0) $3d_{5/2}$, Sb (III) $3d_{5/2}$, Sb(0) $3d_{3/2}$,O 1S, and the Sb(III)$3d_{5/2}$, respectively. The XPS spectrum from the 3:1 Sb2O3: TiO2 showed the presence of 3 peaks which again were deconvolved into 4 peaks. The five peaks were located at 529.8, 530.5 O1S, 531.1, 536.3 and 539.6 eV.

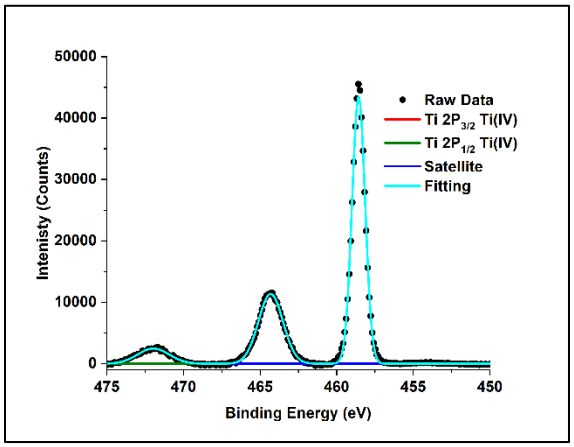

Figure 19. XPS spectrum for hydrothermally synthesized TiO_2 nanoparticles at 175 °C

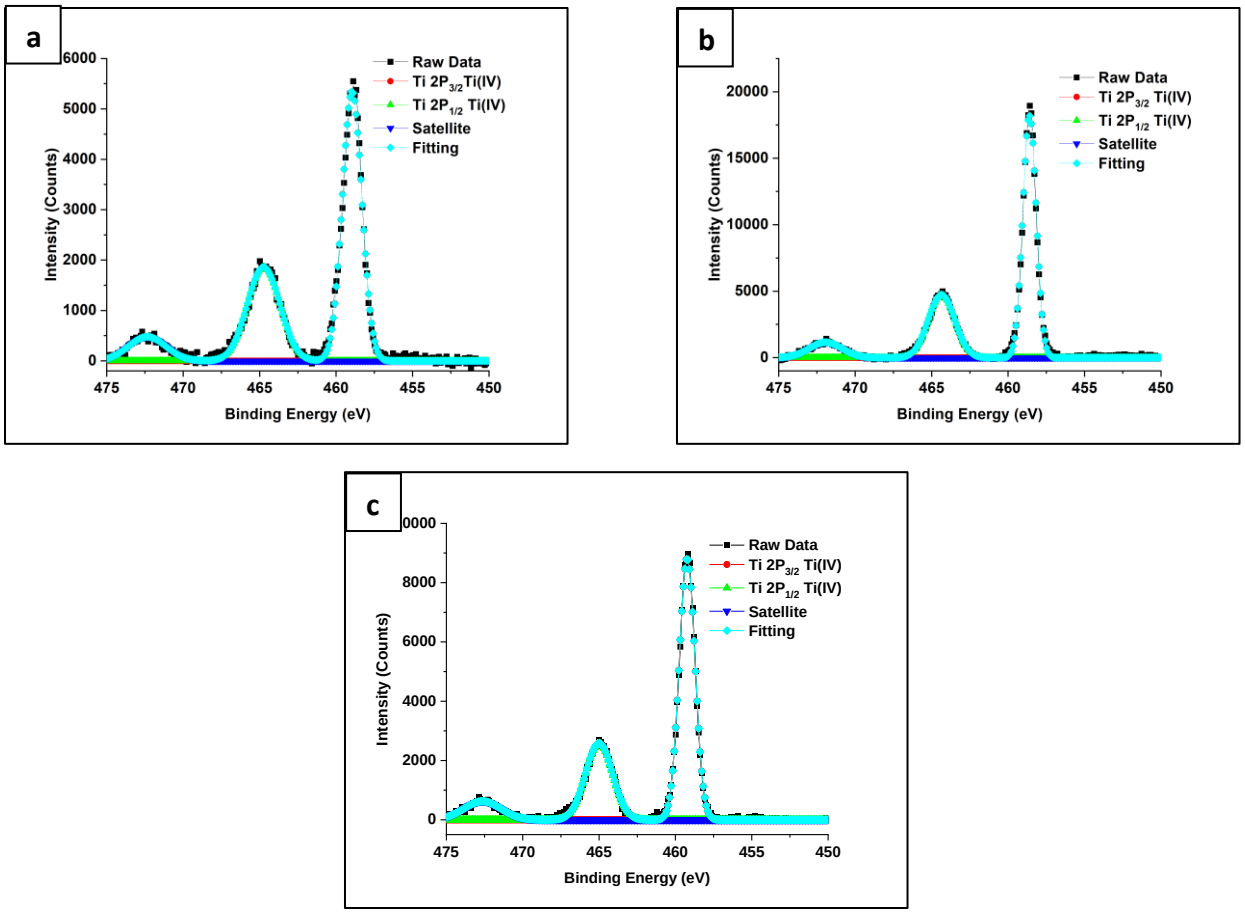

Figure 20. XPS spectrum for Ti2P at (a) 1:1 $TiO_2Sb_2O_3$, (b) 3:1 $TiO_2Sb_2O_3$, and (c) 1:5 $TiO_2Sb_2O_3$

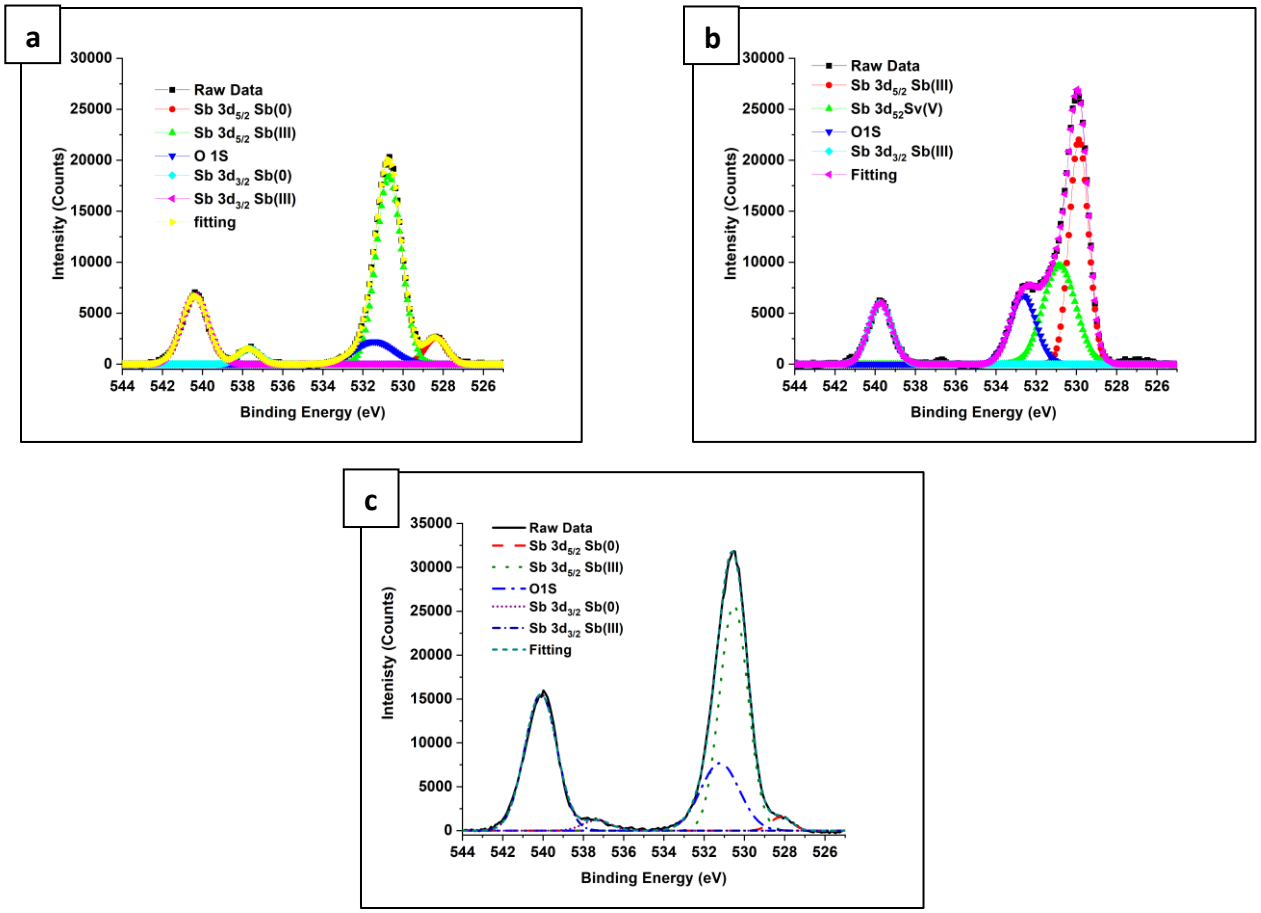

Figure 21. XPS spectrum of Sb 3d and O 1S XPS at (a) 1:5 $TiO_2Sb_2O_3$, (b) 3:1 $TiO_2Sb_2O_3$, and (c) 1:1 $TiO_2Sb_2O_3$

4.1.3 SEM Analysis

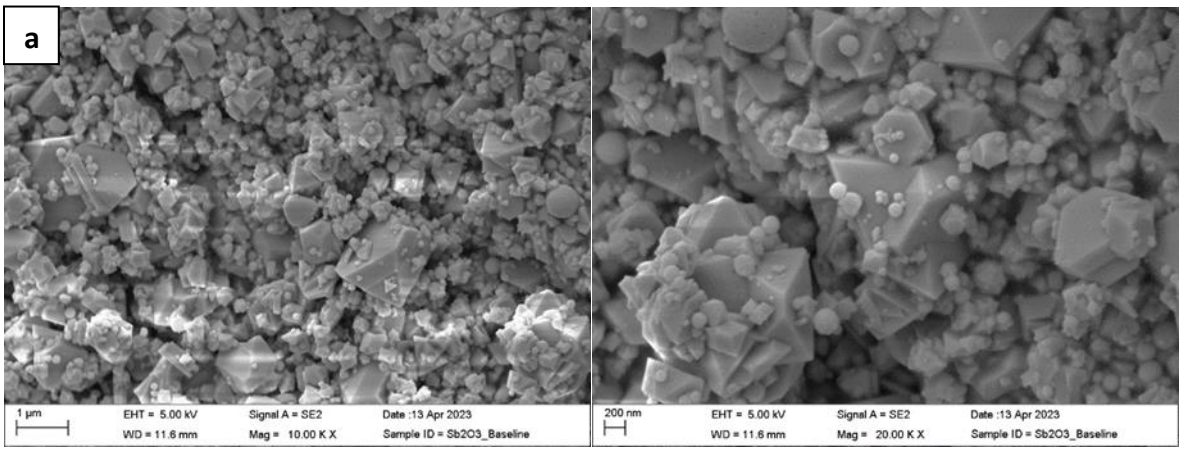

Figure 22. SEM images of (a) Sb2O3 (b) synthesized TiO2 and (c) (3:1) TiO2Sb2O3 material

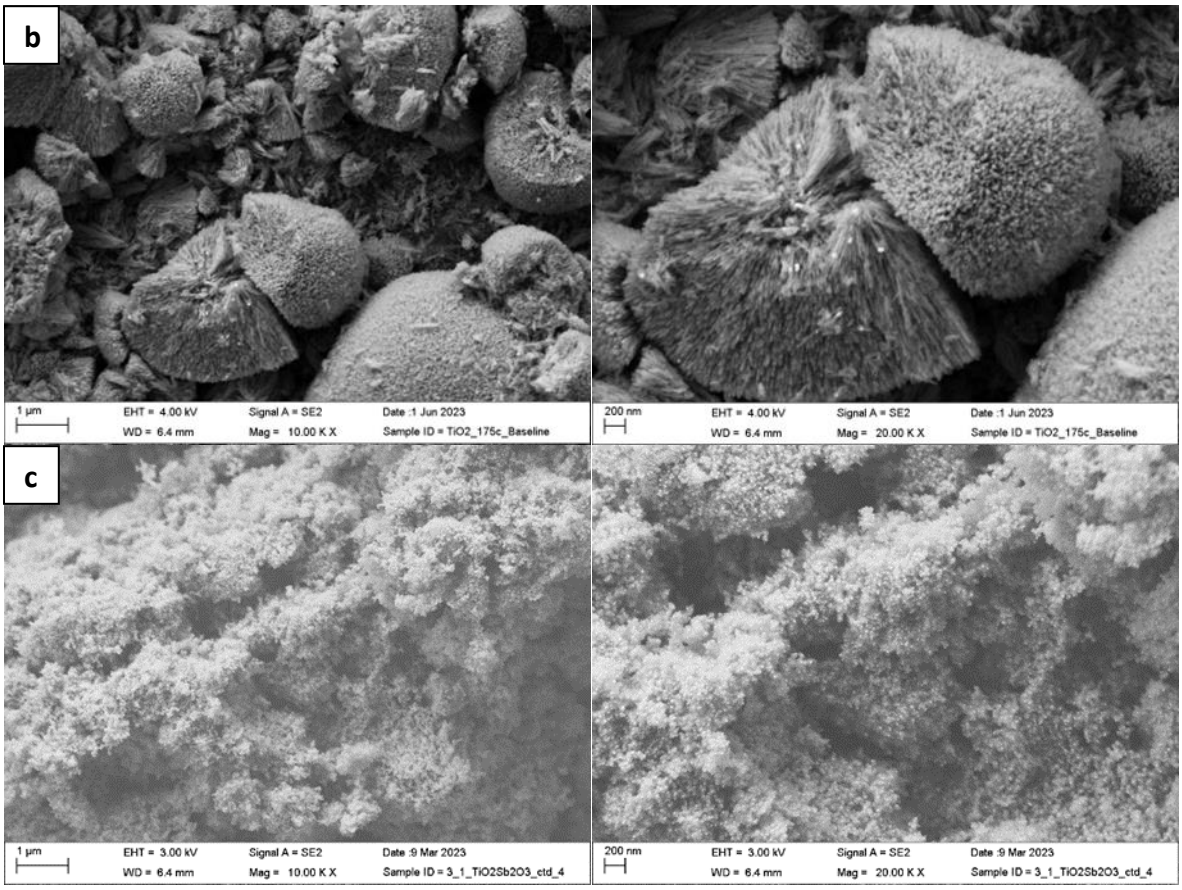

Figure 22, cont.

4.2 Electrochemical Results

Cyclic voltammetry (CV) was performed to investigate the reduction and oxidation processes of the composite material for 5 cycles running at a voltage potential range of 0.05 V – 3.0 V and at a scan rate of 0.1 mVs^{-1}. Figure 25 shows that, during the first cathodic scan three distinctive peaks present at 0.44 V, 1.07 V, and 1.71 V. This can be attributed to the conversion of Sb_2O_3 to metallic Sb and Li_2O (Eq. 1). Furthermore, the solid electrolyte interphase (SEI) layer is known to be irreversible and form during the first cycle since the electrolyte is beginning to deposit onto the electrode surface. It can be presumed that the SEI layer is represented at 1.07 V due to being the sharpest reduction peak followed by an immense decrease in current.

Once it made its first anodic scan, these reduction peaks subsequently minimize and slightly shift towards the right but remain constant and reversible through the next cycles. This shift indicates that the material is gradually activating as lithium insertion is being deposited which simultaneously increases the voltage. Sb is known to have 2 unique peaks at around 1.1 V and 1.4 V during the oxidation scan, distinguishing its elemental conversion of Sb to Sb_2O_3, but with one peak being present at 1.16 V it can be assumed that the TiO_2 overpowered the 1.4 V peak since TiO_2 is seen at 2.03 V with a constant sharp peak. This can also be supported by the mass ratio of TiO_2 being greater in the composite material. This oxidation peak represents the reaction between TiO2 and Li. As for the peak at 2.46 V, it can be assumed it's by the PAN binder. Throughout its scanning process, the $TiO_2Sb_2O_3$ composite demonstrated good electrochemical stability during its charge/discharge due to the constant overlapping of CV scans. The following reversible alloying reaction of Sb_2O_3 as the anode material is shown in Eqs. 1 and 2.[63]

$$Sb2O3 + 6Li+ + 6e- \leftrightarrow 2Sb + 3Li2O \quad (1)$$

$$2Sb + 2xLi+ + 2xe- \leftrightarrow 2LixSb, x \leq 3 \quad (2)$$

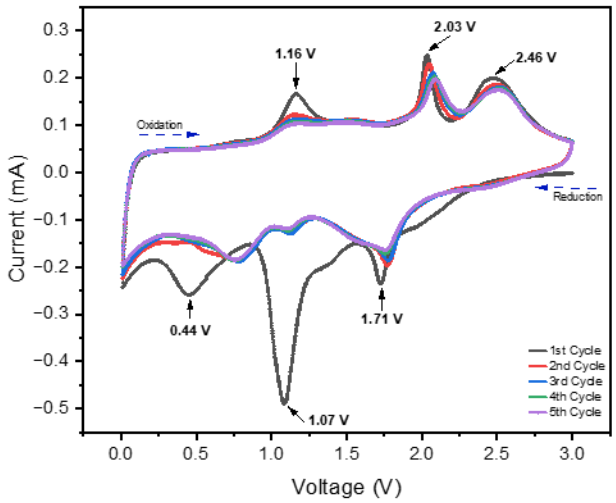

Figure 23. Cyclic Voltammetry curve of the 3:1 $TiO_2Sb_2O_3$ composite material

Another method to evaluate its electrochemical performance as a potential anode material for LIBs is cycle performance. It was scanned at a voltage range of 0.01-3.0 V and a current density of 100 mAg^{-1}. Now there is a unique trend when observing CV and charge/discharge curves. There is a relationship where the concentration profiles coincide with one another based on the points where there are peaks and plateaus.

In Fig. 27c, it begins with a specific capacity of approximately 1,000 $mAhg^{-1}$ due to the significance of the Sb but by the second discharge, it reduced to 624.375 mAh g^{-1} owing to the many factors mentioned before. With calculation it experienced a capacity loss of 35.92% from the 1^{st} cycle to the 2^{nd} cycle, this is related to the development of the SEI layer. Now even though Sb2O3 does occupy a high capacity of 1109 mAhg-1 it does reach the theoretical capacity of Sb at 660 mAhg-1 which is a good sign. As observed from Fig. 27c, there are plateaus close to 1.75 V and 1.12 V during the first discharge curve of the composite material. This is tied to the reduction peaks seen in Fig. 25 during the first cycle. These plateaus are related to the conversion of Sb_2O_3 to Sb and Li^+ becoming Li_2O as well as the creation of the SEI layer as Li^+ is being inserted causing an irreversible capacity between the first two discharges. Now at the first charge, there are peaks roughly at 2.0 V and 2.4 V which resemble to the peaks seen in Fig.25 along the oxidation scan, which demonstrates the release of the Li^+ ions received from the discharge and making the Sb oxidized to Sb_2O_3. Therefore, these plateaus and peaks demonstrate chemical reactions that are occurring as its being charged/discharged.

At the beginning of its sequence, a charged cycle took 6 hours 5 min and 6 hours 9 min to discharge. Now by its 100^{th} cycle it took 5 hours 22 min to charge and 5 hours 25 min to

discharge. It decreased overtime with just one hour. Therefore, to complete 100 cycles it approximately took a total of 45-50 days.

From the 50^{th} cycle to the 100^{th} cycle there was very good signs of stability due to the overlapping of the curves. Through calculation, it experienced just 2.90% capacity loss. There is an assumption that the capacity can increase overtime since there is a slight of increase in capacity at the 100^{th} cycle. This is a characteristic of Titanium (Ti) that it stores more power as it's been cycling which increases its lifespan at a steady rate. This action is also represented on the cycle performance of TiO_2 (Fig. 27b). Whereby the 100^{th} cycle, it had a higher specific capacity than what it was at the 2^{nd} cycle. Due to this, the following test of the $TiO_2Sb_2O_3$ composite material will continue scanning unto 500 cycles. Both the synthesized TiO2 material and Sb_2O_3 were tested to create a baseline. The pure Sb_2O_3 (Fig.27a) displays the highest specific capacity out of the three at the initial few cycles. But unfortunately, by the 25^{th} cycle of the pure Sb_2O_3 there is a rapid decrease of the specific capacity where it exhibits instability and signs of decay as it progresses. Which proves one of the main concerns of Sb. The distance between the 1^{st} and 2^{nd} cycle you can predict the size of the SEI layer which is small but what hinders the performance is the pulverization that occurs as lithium is being deposited onto the surface.

As for TiO_2 its cycle performance demonstrated excellent stability and reversibility. Beginning with approximately 375 mAhg-1 and dropping to 160 mAhg-1 in the second cycle. Undergoing a capacity loss of 55.54%. Yet by the 25^{th} cycle, it was increasing in capacity gradually as it was reaching its 100^{th} cycle.

In comparison to the three charge/discharge profiles, the Sb profile shows wide gaps meaning loss of stability while the synthesized material looks similar to TiO_2. Justifying that just with the pattern of the profiles one can distinguish that the incorporation of TiO_2 was significant.

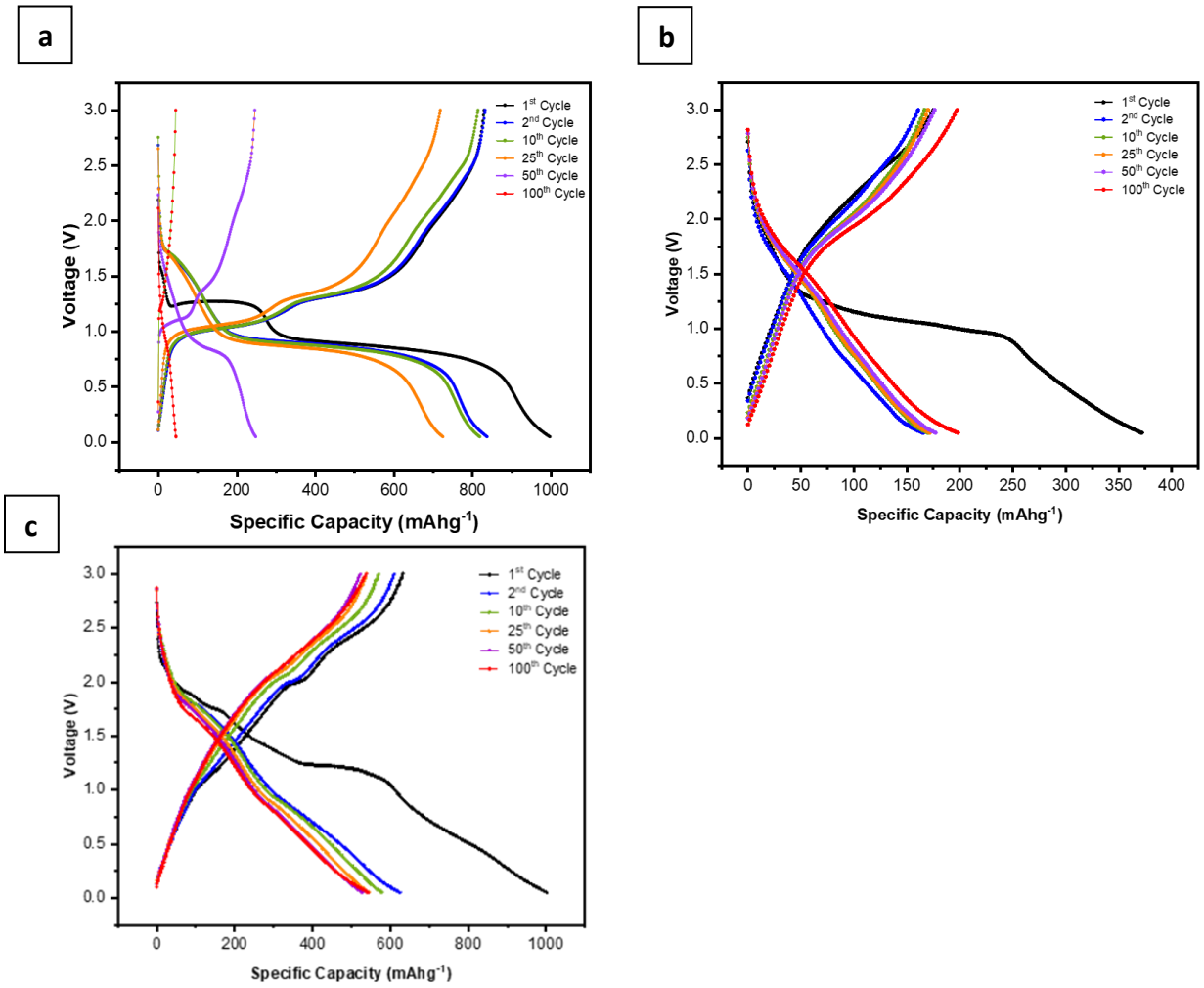

Figure 24. Charge/Discharge curves at 100 cycles of (a) Sb_2O_3 (b) TiO_2 (c) (3:1) $TiO_2Sb_2O_3$

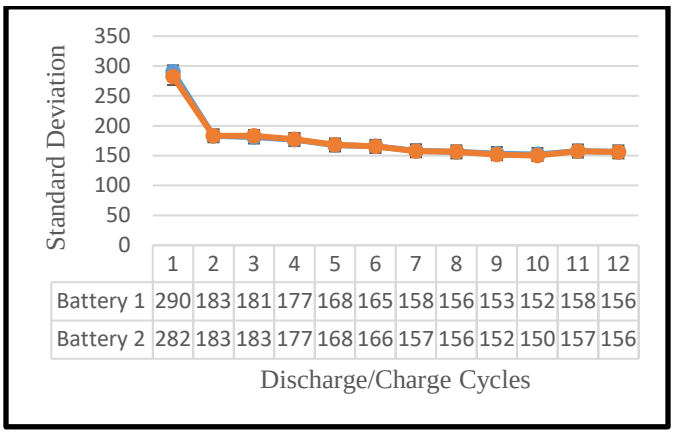

Figure 25. Standard deviation and error bars of (3:1) $TiO_2Sb_2O_3$

To continue with the investigation on the cycle performance, the specific capacity was plotted against the total of cycle numbers, Fig.29. During this test, a current density of 100 $mAhg^{-1}$ for 100 cycles under a potential of 0.05 to 3.0 V. It can be observed that the of TiO_2 tremendously helped with the stability of Sb_2O_3 having better cycling. It mitigated the large volume expansion that occurs during delithiation/lithiation which led to improving the amount of capacity it can retain throughout its life cycle. By the 40^{th} cycle it reached its stability point of approximately 523 $mAhg^{-1}$ which is over the traditional capacity of graphite. Based off Han et al. its composite material reached stabilization until after 60 cycles and dealt with an approximation of 40% capacity loss from its initial specific capacity of 1021 $mAhg^{-1}$ to its stable state.

$TiO_2Sb_2O_3$ did exhibit an initial capacity of 632 $mAhg^{-1}$ and experienced a capacity loss of 35% during its first discharge. But throughout its life cycle it was steady with minimal changes of less than 5 $mAhg^{-1}$ from the 40^{th} to 80^{th} cycle. At the 77^{th} cycle its specific capacity was beginning to increase with it being 521 $mAhg^{-1}$ and by the 100^{th} cycle it was at 536 $mAhg^{-1}$. Yet Sb_2O_3 experienced an extreme amount of capacity loss right before reaching the 20^{th} cycle

and by 60th cycle it had a specific capacity less than 100 $mAhg^{-1}$. It can be assumed that the thickness of the coating along Sb_2O_3 was significant to act as buffer while undergoing volume changes.

Based on figure 16, standard deviation of their specific capacities was calculated on two lithium-ion batteries of (3:1) $TiO_2Sb_2O_3$. Data was to determine if results were consistent and show confidence levels by including error bars. Standard deviations were computed and compared for each discharge/charge for 100 cycles. At the first discharge of both batteries, it evaluated a standard deviation of 290 and 282 respectively, showing an overlap of the error bars. This statement of overlapping is represented along all the data. This demonstrates that the difference of each value set was not statistically significant. Which supports that the following anode nanocomposite material is reliable for lithium-ion battery usage.

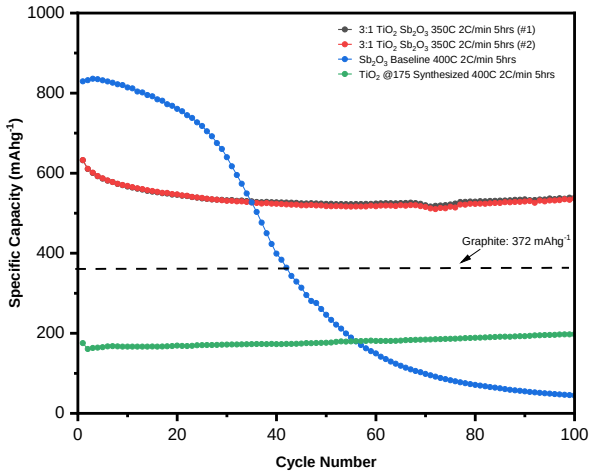

Figure 26. Charge profiles of designated materials

Lastly to study the electrochemical properties of $TiO_2Sb_2O_3$ composite material, EIS measurements were presented in comparison to its parent material as seen on Fig. 30a. When evaluating the Nyquist plots, its divided into two fragments: a semi-circle and tail. It begins

scanning left to right, at the formation of the semi-circle to the tail. Left being at a high frequency and completes at a low frequency. The shape of the semi-circle is attributed to the distribution of Li^+ ions as it reaches the surface of the electrolyte interface and the amount of resistance it experiences during the exchange of charges as the electrode and electrolyte make contact. The diameter of the semi-circle relates to the amount of resistance its undergoing. Therefore, the larger it is the more resistance. A prominent cause of impedance increase can be related to high temperature, lithium plating, SEI formation, or volume loss of electrolyte which will dry local areas between the electrodes. These issues are highly concentrated towards the negative electrode. Now at the segment of the tail, its related to the diffusion of Li^+ ions towards the active material. These EIS measurements were converted to be displayed as an equivalent circuit as seen on Fig. 30b. The following components are R_p, R_s, W and constant phase element (*CPE*). In its respected order, the first component corresponds to the polarization resistance which is the restraint of charge transfer between the electrolyte and the electrode. The solution resistance is the resistance between both electrodes present. The Warburg impedance coefficient at high frequencies is usually represented as a small number because the diffusing reactants don't necessarily travel far. Yet at low frequencies, the Warburg impedance increases since its expected for the reactants to disperse far. And lastly the constant phase element reflects the behavior of a double layer. Based on the Nyquist plots, the Sb_2O_3 baseline had a resistance of 163 Ω, synthesized TiO_2 100 Ω, and $TiO_2Sb_2O_3$ composite material an overall resistance between 90-110 Ω from the three trials. The resistance overall improved significantly being close to the resistance that TiO_2 displays. This indicates that there was a smoother diffusion of Li^+ ions between the electrodes and electrolyte. The following frequency values for R_p, *Rs*, and W were roughly in range of 0.1 Hz and 100 Hz for all anodes tested as seen on Fig #a and b.

On Fig#, the tail portion from the Nyquist plots seen on Fig#a were fitted and plotted as $Z^{'}$ *vs* $\omega^{-1/2}$ to determine the Warburg coefficient (σ). This coefficient is given through the slope of the fitted line. Where $Z^{'}$ is impedance in the unit of ohms and ω the angular frequency.

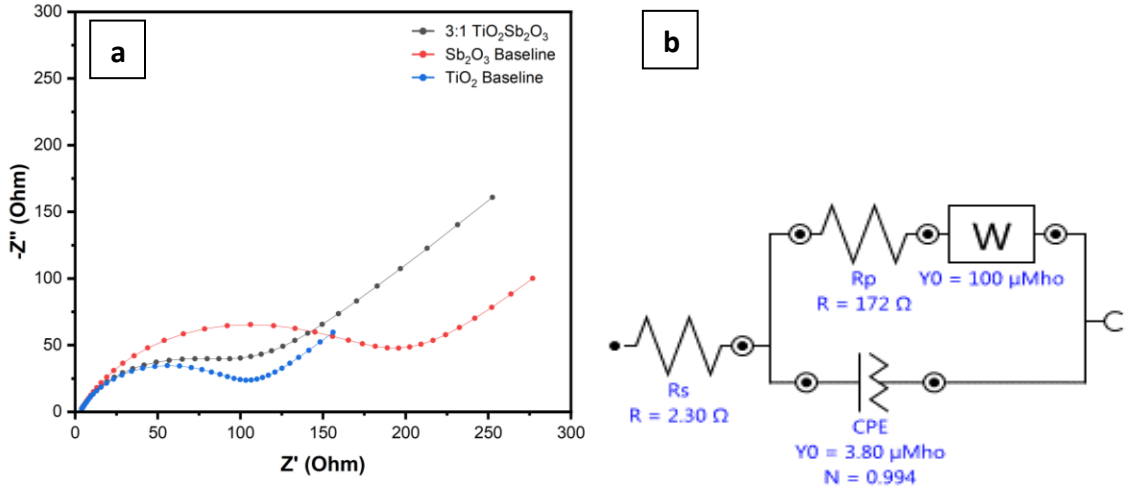

Figure 27. (a) Nyquist plots of (3:1) $TiO_2Sb_2O_3$ against parent material and (b) its equivalent circuit

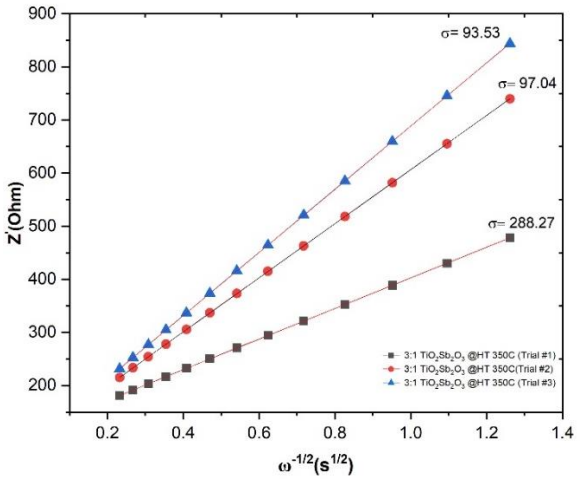

Figure 28. Warburg coefficients from Nyquist plot of (3:1) TiO2Sb2O3 material

To examine its rate compatibility each material was tested at different densities of 50,100,200,400, 500 and back to 50 mAg^{-1} at a voltage range of 0.01 to 3.0 V. As seen on Fig. 32, both parent materials were compared to both testing's of (3:1) $TiO_2Sb_2O_3$ and the synthesized material surpassed them significantly. The Sb_2O_3 showed that at low densities it

retained more capacity but as the density was increasing from 100 to 500 mAg^{-1} it was exponentially decreasing. As it reached back to 50 mAg^{-1} it started at a high capacity but automatically reduced. Yet TiO_2 had 100% reversibility with great signs of steadiness even though it had the lowest capacity. In contrast to the (3:1) $TiO_2Sb_2O_3$ it retained the most capacity out of the three, at the highest density of 500 mAg^{-1} with a capacity roughly at 330 $mAhg^{-1}$. But most importantly at a density of 50 mAg^{-1} at the beginning and end of its life cycle it exhibited great reversibility properties. At the end of its 10 cycles at the beginning, it had a capacity of 354 and 312 mAg^{-1} and finishing off at 336 and 281 mAg^{-1} respectively for both trails. This certainly confirms that the composite material can be considered as a potential anode material.

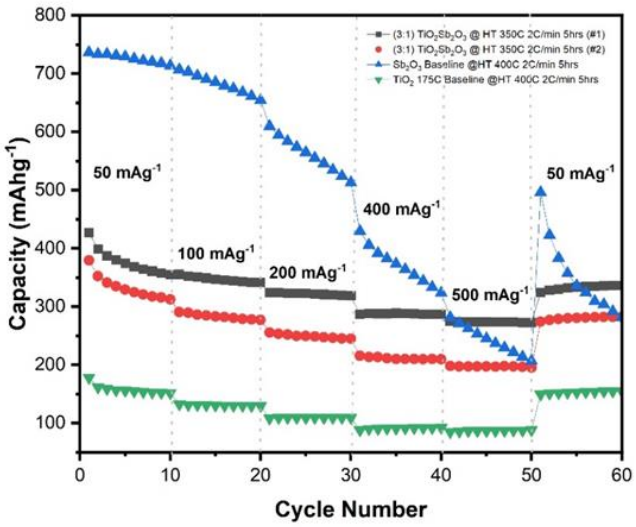

Figure 29. Rate performance of (3:1) $TiO_2Sb_2O_3$ and baseline materials at different current densities.

CHAPTER V

CONCLUSION

In conclusion $TiO_2Sb_2O_3$ was successfully fabricated through the hydrolysis of $TiCl_4$ at a hydrothermal treatment at 175°C. This process is safe and time efficient compared to the other methods performed.

Due to results given on annealed material, unannealed process was favored. With that in perspective the methodology changed to performing hydrolysis and hydrothermal instead. With this change data was significantly improved in its performance. Continuing with hydrolysis/hydrothermal procedure, $TiO_2Sb_2O_3$ was synthesized at different ratios of: (1:1), (1:5), and (3:1) with applied heat treatments at 300°C, 350°C, 400°C, 450°C. Based on their electrochemical performances, the (3:1) ratio at 350°C displayed the best stability qualities and retention results. This is feasible due to the addition of TiO_2 applying those characteristics. Additional electrochemical results will be included in the appendix. A runner-up based on its electrochemical performance is (3:1) $TiO_2Sb_2O_3$ heat treated at 400°C which displayed a steady rate and average capacity based on fig. 28 and fig. 29, but when observing its cyclic voltammetry there were no distinct peaks representing Sb just a noticeable peak of Ti which may have overpowered the Sb peaks. Also, its capability of retaining capacity was not high compared to material that was heat treated at 350°C. Overall performing slurry coated anodes is more

efficient and expedited compared to centrifugal spinning. Issues dealt when calcinating Sb-precursor fibers was experiencing huge shrinkage leaving no material to work with. Optimizing this process was necessary and required to progress on making precursor-based fibers to calcinate.

Overall (3:1) TiO_2/Sb_2O_3 nanocomposite delivered excellent cycling stability and rate capability when applied as an anode material for LIBs. The TiO_2 eased the large volume change that occurs in Sb_2O_3 due to its good structural stability and low volume expansion (10%). Based on electrochemical performance, TiO_2/Sb_2O_3 executed the best qualities from both TiO_2 and Sb_2O_3 offers, it's high capacity and steady rate. Based on halfway its cycle-life, it executed an overall loss of 2.9% at its final cycle. The development of TiO_2 /Sb_2O_3 nanocomposites demonstrates as a promising candidate for the next generation of lithium-ion batteries.

REFERENCES

[1] V. S. Bagotsky, "Fuel cells, batteries, and the development of electrochemistry," *Journal of Solid State Electrochemistry,* vol. 15, no. 7-8, pp. 1559-1562, 2011.

[2] B. Scrosati, "History of lithium batteries," *Journal of solid state electrochemistry,* vol. 15, no. 7-8, pp. 1623-1630, 2011.

[3] F. Schipper and D. Aurbach, "A brief review: past, present and future of lithium ion batteries," *Russian Journal of Electrochemistry,* vol. 52, pp. 1095-1121, 2016.

[4] G. E. Blomgren, "The development and future of lithium ion batteries," *Journal of The Electrochemical Society,* vol. 164, no. 1, p. A5019, 2016.

[5] S. Panero, B. Scrosati, M. Wachtler, and F. Croce, "Nanotechnology for the progress of lithium batteries R&D," *Journal of power sources,* vol. 129, no. 1, pp. 90-95, 2004.

[6] K. Wong and S. Dia, "Nanotechnology in batteries," *Journal of energy resources technology,* vol. 139, no. 1, 2017.

[7] R. Moshtev and B. Johnson, "State of the art of commercial Li ion batteries," *Journal of power sources,* vol. 91, no. 2, pp. 86-91, 2000.

[8] J. Lu, Z. Chen, Z. Ma, F. Pan, L. A. Curtiss, and K. Amine, "The role of nanotechnology in the development of battery materials for electric vehicles," *Nature nanotechnology,* vol. 11, no. 12, pp. 1031-1038, 2016.

[9] H. Zhang, X. Sun, X. Zhang, H. Lin, K. Wang, and Y. Ma, "High-capacity nanocarbon anodes for lithium-ion batteries," *Journal of Alloys and Compounds,* vol. 622, pp. 783-788, 2015.

[10] L. Ji, Z. Lin, M. Alcoutlabi, and X. Zhang, "Recent developments in nanostructured anode materials for rechargeable lithium-ion batteries," *Energy & Environmental Science,* vol. 4, no. 8, pp. 2682-2699, 2011.

[11] C. Liang, M. Gao, H. Pan, Y. Liu, and M. Yan, "Lithium alloys and metal oxides as high-capacity anode materials for lithium-ion batteries," *Journal of alloys and compounds,* vol. 575, pp. 246-256, 2013.

[12] Z. Xing *et al.*, "One-pot hydrothermal synthesis of Nitrogen-doped graphene as high-performance anode materials for lithium ion batteries," *Scientific reports,* vol. 6, no. 1, pp. 1-10, 2016.

[13] H. Li and H. Zhou, "Enhancing the performances of Li-ion batteries by carbon-coating: present and future," *Chemical Communications,* vol. 48, no. 9, pp. 1201-1217, 2012.

[14] X. Zhang, L. Ji, O. Toprakci, Y. Liang, and M. Alcoutlabi, "Electrospun nanofiber-based anodes, cathodes, and separators for advanced lithium-ion batteries," *Polymer Reviews,* vol. 51, no. 3, pp. 239-264, 2011.

[15] H. Lund, "Renewable energy strategies for sustainable development," *energy,* vol. 32, no. 6, pp. 912-919, 2007.

[16] F. Duffner, M. Wentker, M. Greenwood, and J. Leker, "Battery cost modeling: A review and directions for future research," *Renewable and Sustainable Energy Reviews,* vol. 127, p. 109872, 2020.

[17] J. Janek and W. G. Zeier, "A solid future for battery development," *Nature Energy,* vol. 1, no. 9, pp. 1-4, 2016.

[18] T. Kim, W. Song, D.-Y. Son, L. K. Ono, and Y. Qi, "Lithium-ion batteries: outlook on present, future, and hybridized technologies," *Journal of materials chemistry A,* vol. 7, no. 7, pp. 2942-2964, 2019.

[19] B. Scrosati and J. Garche, "Lithium batteries: Status, prospects and future," *Journal of power sources,* vol. 195, no. 9, pp. 2419-2430, 2010.

[20] M. Wakihara, "Recent developments in lithium ion batteries," *Materials Science and Engineering: R: Reports,* vol. 33, no. 4, pp. 109-134, 2001.

[21] J. Xie and Y.-C. Lu, "A retrospective on lithium-ion batteries," *Nature Communications,* vol. 11, no. 1, p. 2499, 2020/05/19 2020, doi: 10.1038/s41467-020-16259-9.

[22] J.-M. Tarascon and M. Armand, "Issues and challenges facing rechargeable lithium batteries," *nature,* vol. 414, no. 6861, pp. 359-367, 2001.

[23] H. Zhang, Y. Yang, D. Ren, L. Wang, and X. He, "Graphite as anode materials: Fundamental mechanism, recent progress and advances," *Energy Storage Materials,* vol. 36, pp. 147-170, 2021.

[24] J. Shim and K. A. Striebel, "The dependence of natural graphite anode performance on electrode density," *Journal of power sources,* vol. 130, no. 1-2, pp. 247-253, 2004.

[25] P. Poizot, S. Laruelle, S. Grugeon, L. Dupont, and J. Tarascon, "Searching for new anode materials for the Li-ion technology: time to deviate from the usual path," *Journal of Power Sources,* vol. 97, pp. 235-239, 2001.

[26] C. Curry, "Lithium-ion battery costs and market," *Bloomberg New Energy Finance,* vol. 5, no. 4-6,

p. 43, 2017.

[27] C. Vaalma, D. Buchholz, M. Weil, and S. Passerini, "A cost and resource analysis of sodium-ion batteries," *Nature reviews materials,* vol. 3, no. 4, pp. 1-11, 2018.

[28] C. J. Orendorff, "The role of separators in lithium-ion cell safety," *The Electrochemical society interface,* vol. 21, no. 2, p. 61, 2012.

[29] M. V. Reddy, A. Mauger, C. M. Julien, A. Paolella, and K. Zaghib, "Brief history of early lithium-battery development," *Materials,* vol. 13, no. 8, p. 1884, 2020.

[30] S. S. Zhang, "Liquid electrolyte lithium/sulfur battery: Fundamental chemistry, problems, and solutions," *Journal of Power Sources,* vol. 231, pp. 153-162, 2013.

[31] Y. S. Meng, V. Srinivasan, and K. Xu, "Designing better electrolytes," *Science,* vol. 378, no. 6624,

p. eabq3750, 2022.

[32] Y. K. Liu, C. Z. Zhao, J. Du, X. Q. Zhang, A. B. Chen, and Q. Zhang, "Research Progresses of Liquid Electrolytes in Lithium-Ion Batteries," *Small,* vol. 19, no. 8, p. 2205315, 2023.

[33] K. Xu, "Li-ion battery electrolytes," *Nature Energy,* vol. 6, no. 7, pp. 763-763, 2021.

[34] C. Wang *et al.*, "Lithium difluorophosphate as a promising electrolyte lithium additive for high-voltage lithium-ion batteries," *ACS applied energy materials,* vol. 1, no. 6, pp. 2647-2656, 2018.

[35] A. Mauger, C. M. Julien, J. B. Goodenough, and K. Zaghib, "Tribute to Michel Armand: from rocking chair–Li-ion to solid-state lithium batteries," *Journal of The Electrochemical Society,* vol. 167, no. 7, p. 070507, 2019.

[36] I. D. Campbell, M. Marzook, M. Marinescu, and G. J. Offer, "How observable is lithium plating? Differential voltage analysis to identify and quantify lithium plating following fast charging of cold lithium-ion batteries," *Journal of the electrochemical society,* vol. 166, no. 4, pp. A725-A739, 2019.

[37] A. H. Zimmerman and M. V. Quinzio, "Lithium plating in lithium-ion cells," in *NASA Battery Workshop*, 2010, vol. 16, p. 18.

[38] L. A. Riley *et al.*, "Conformal surface coatings to enable high volume expansion Li-ion anode materials," *ChemPhysChem,* vol. 11, no. 10, pp. 2124-2130, 2010.

[39] P. Bai, J. Li, F. R. Brushett, and M. Z. Bazant, "Transition of lithium growth mechanisms in liquid electrolytes," *Energy & Environmental Science,* vol. 9, no. 10, pp. 3221-3229, 2016.

[40] M. Safari, M. Morcrette, A. Teyssot, and C. Delacourt, "Multimodal physics-based aging model for life prediction of Li-ion batteries," *Journal of The Electrochemical Society,* vol. 156, no. 3, p. A145, 2008.

[41] G. Liu and W. Lu, "A model of concurrent lithium dendrite growth, SEI growth, SEI penetration and regrowth," *Journal of The Electrochemical Society,* vol. 164, no. 9, p. A1826, 2017.

[42] B. Moradi and G. G. Botte, "Recycling of graphite anodes for the next generation of lithium ion batteries," *Journal of Applied Electrochemistry,* vol. 46, pp. 123-148, 2016.

[43] J. Nanda, S. K. Martha, and R. Kalyanaraman, "High-capacity electrode materials for electrochemical energy storage: Role of nanoscale effects," *Pramana,* vol. 84, pp. 1073-1086, 2015.

[44] J. P. Pender *et al.*, "Electrode degradation in lithium-ion batteries," *ACS nano,* vol. 14, no. 2, pp. 1243-1295, 2020.

[45] P. Zheng *et al.*, "Microstructure Engineered Silicon Alloy Anodes for Lithium-Ion Batteries: Advances and Challenges," *Batteries & Supercaps,* vol. 6, no. 1, p. e202200481, 2023.

[46] C. Zhang *et al.*, "Challenges and recent progress on silicon-based anode materials for next-generation lithium-ion batteries," *Small Structures,* vol. 2, no. 6, p. 2100009, 2021.

[47] Y. Xu, J. Guo, and C. Wang, "Sponge-like porous carbon/tin composite anode materials for lithium ion batteries," *Journal of Materials Chemistry,* vol. 22, no. 19, pp. 9562-9567, 2012.

[48] X. Zhao *et al.*, "Electrochemical properties of some Sb or Te based alloys for candidate anode materials of lithium-ion batteries," *Journal of alloys and compounds,* vol. 315, no. 1-2, pp. 265-269, 2001.

[49] J. He, Y. Wei, T. Zhai, and H. Li, "Antimony-based materials as promising anodes for rechargeable lithium-ion and sodium-ion batteries," *Materials Chemistry Frontiers,* vol. 2, no. 3, pp. 437-455, 2018.

[50] S. Liang, Y. J. Cheng, J. Zhu, Y. Xia, and P. Müller-Buschbaum, "A chronicle review of nonsilicon
(Sn, Sb, Ge)-based lithium/sodium-ion battery alloying anodes," *Small Methods,* vol. 4, no. 8, p. 2000218, 2020.

[51] R. Amine *et al.*, "A practical phosphorus-based anode material for high-energy lithium-ion batteries," *Nano Energy,* vol. 74, p. 104849, 2020.

[52] X. Jiao *et al.*, "Crumpled nitrogen-doped graphene-wrapped phosphorus composite as a promising anode for lithium-ion batteries," *ACS applied materials & interfaces,* vol. 11, no. 34, pp. 30858-30864, 2019.

[53] Z. Yue *et al.*, "Utilizing a graphene matrix to overcome the intrinsic limitations of red phosphorus as an anode material in lithium-ion batteries," *Carbon,* vol. 127, pp. 588-595, 2018.

[54] H. Hou *et al.*, "NiSb alloy hollow nanospheres as anode materials for rechargeable lithium ion batteries," *Chemical Communications,* vol. 50, no. 60, pp. 8201-8203, 2014.

[55] F.-S. Ke *et al.*, "Three-dimensional nanoarchitecture of Sn–Sb–Co alloy as an anode of lithium-ion batteries with excellent lithium storage performance," *Journal of Materials Chemistry,* vol. 22, no. 34, pp. 17511-17517, 2012.

[56] J. Liu *et al.*, "New nanoconfined galvanic replacement synthesis of hollow Sb@ C yolk–shell spheres constituting a stable anode for high-rate Li/Na-ion batteries," *Nano Letters,* vol. 17, no. 3, pp. 2034-2042, 2017.

[57] H. Bryngelsson, J. Eskhult, L. Nyholm, M. Herranen, O. Alm, and K. Edström, "Electrodeposited Sb and Sb/Sb2O3 nanoparticle coatings as anode materials for Li-ion batteries," *Chemistry of materials,* vol. 19, no. 5, pp. 1170-1180, 2007.

[58] T. Ramireddy, M. M. Rahman, T. Xing, Y. Chen, and A. M. Glushenkov, "Stable anode performance of an Sb–carbon nanocomposite in lithium-ion batteries and the effect of ball milling mode in the course of its preparation."

[59] Y. Tan, L. Chen, H. Chen, Q. Hou, and X. Chen, "Synthesis of a symmetric bundle-shaped Sb2O3 and its application for anode materials in lithium ion batteries," *Materials Letters,* vol. 212, pp.
103-106, 2018.

[60] Y. Liu *et al.*, "Enhanced electrochemical performance of Sb2O3 as an anode for lithium-ion batteries by a stable cross-linked binder," *Applied Sciences,* vol. 9, no. 13, p. 2677, 2019.

[61] S. Yoon and A. Manthiram, "Sb-MO x-C (M= Al, Ti, or Mo) nanocomposite anodes for lithium-ion batteries," *Chemistry of Materials,* vol. 21, no. 16, pp. 3898-3904, 2009.

[62] N. Nitta and G. Yushin, "High-capacity anode materials for lithium-ion batteries: choice of elements and structures for active particles," *Particle & Particle Systems Characterization,* vol. 31, no. 3, pp. 317-336, 2014.

[63] H. Li *et al.*, "The different Li/Na ion storage mechanisms of nano Sb2O3 anchored on graphene," *Journal of Power Sources,* vol. 385, pp. 114-121, 2018.

[64] R. Eichler, "The periodic table of elements: superheavy in chemistry," *Nuclear Physics News,* vol. 29, no. 1, pp. 11-15, 2019.

[65] A. Darwiche, C. Marino, M. T. Sougrati, B. Fraisse, L. Stievano, and L. Monconduit, "Better cycling performances of bulk Sb in Na-ion batteries compared to Li-ion systems: an unexpected electrochemical mechanism," *Journal of the American Chemical Society,* vol. 134, no. 51, pp. 20805-20811, 2012.

[66] W.-J. Zhang, "Lithium insertion/extraction mechanism in alloy anodes for lithium-ion batteries," *Journal of Power Sources,* vol. 196, no. 3, pp. 877-885, 2011.

[67] M. Hu, Y. Jiang, W. Sun, H. Wang, C. Jin, and M. Yan, "Reversible conversion-alloying of Sb2O3 as a high-capacity, high-rate, and durable anode for sodium ion batteries," *ACS applied materials & interfaces,* vol. 6, no. 21, pp. 19449-19455, 2014.

[68] G. W. Morey, "Hydrothermal synthesis," *Journal of the American Ceramic Society,* vol. 36, no. 9, pp. 279-285, 1953.

[69] K. Sarkar *et al.*, "Electrospinning to forcespinning™," *Materials today,* vol. 13, no. 11, pp. 12-14, 2010.

[70] A. Miranda *et al.*, "A comprehensive study of hydrolyzed polyacrylamide as a binder for silicon anodes," *ACS applied materials & interfaces,* vol. 11, no. 47, pp. 44090-44100, 2019.

APPENDIX

APPENDIX

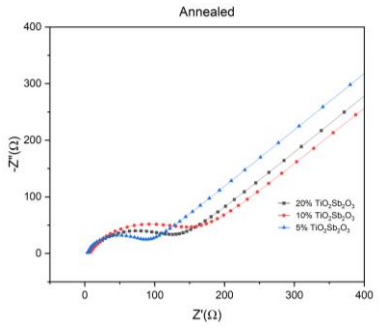

Figure 30. Impedance of annealed nanocomposite

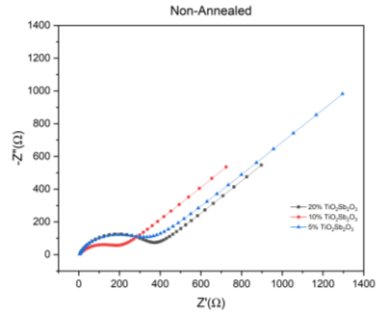

Figure 31. Impedance of non-annealed nanocomposite

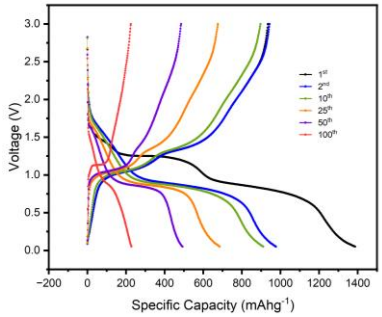

Figure 32. Discharge/Charge of 5% TiO2Sb2O3 non-annealed

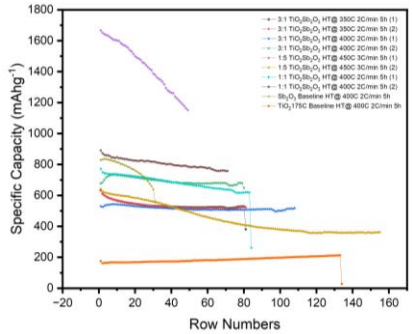

Figure 33. Charge profiles of TiO2Sb2O3 at different ratios

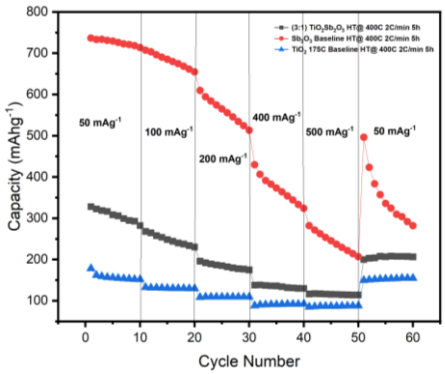

Figure 34. Rate performance of 3:1 TiO2Sb2O3 at 400

BIOGRAPHICAL SKETCH

Student's full name is Kithzia Czarina Gomez. She attended the University of Texas Rio Grande Valley to obtain both her undergraduate and graduate degrees. She received her Bachelor of Science in Chemistry in Spring 2019, and her Master of Science in Mechanical Engineering with a concentration on Materials Science in July 2023. She can be reached at kgomez1208@yahoo.com.